# Enhancing Electrogenerated Chemiluminescence through Triplet State Dynamics

Jiajia Gao,[a] Badma Dylykov,[a, b] Zelong Li,[a] Sherwin Chong Li Tan,[a] Feng Liu,[a] Veronica Gurung,[a] and Le Yang*[a, c]

*a Institute of Materials Research and Engineering (IMRE), Agency for Science, Technology and Research (A*STAR), 2 Fusionopolis Way, Innovis #08-03, Singapore 138634, Republic of Singapore*
*b Department of Chemistry, National University of Singapore, 117543, Singapore*
*c Department of Materials Science & Engineering, National University of Singapore, 117575, Singapore*

## Abstract

Electrogenerated chemiluminescence (ECL) has attracted considerable interest for its applications in highly sensitive bioanalysis and emerging light-emitting display technologies, owing to its high signal-to-noise ratio, spatial precision, and controllable emission. The electrochemical generation of excitons through anion–cation annihilation enables the efficient formation of triplet states, offering an intrinsic quantum yield of up to 75% and allowing for low operating potentials. These characteristics make ECL systems inherently brighter and more energy efficient. Motivated by these advantages, this review focuses on the role of triplet-state dynamics in advancing ECL technologies. We detail the mechanistic pathways by which triplet excitons enhance annihilation-type ECL, covering foundational work on triplet–triplet annihilation (TTA) and recent developments in thermally activated delayed fluorescence (TADF), triplet–triplet energy transfer (TTET), and related mechanisms. Key characterization techniques and theoretical models used to identify and understand triplet-state involvement are summarized. Furthermore, we categorize major classes of triplet-based ECL luminophores—including metal complexes, organic molecules, and emerging nanostructures, with an emphasis on their structure–function relationships. Finally, we review current applications of triplet-functionalized ECL systems and outline the challenges and opportunities that lie ahead, highlighting the importance of continued research to fully exploit the potential of triplet-state processes in ECL.

## 1. Introduction

Electrochemiluminescence (ECL), also known as electrogenerated chemiluminescence, is a light-emitting phenomenon induced by electrochemical reactions. It combines the high sensitivity of chemiluminescence with the spatial and temporal control of electrochemistry, making it a versatile tool for a wide range of applications. Since its discovery by Hoijtink and co-workers, who first reported in 1963 the electro-generated chemiluminescent reaction between anthracene's positive and negative radical ions,[1] ECL has gained significant attention in early-stage research and then emerging application in biosensing, medical diagnostics, material science, and display technologies with its high sensitivity and tunability due to high-contrast visualization with minimal background interference.[2-4]

The ECL process typically involves three consecutive steps: 1) the electrochemical generation of radical ion intermediates, 2) ion diffusion and electron transfer reactions to form excited-state species 3) energy transfer and emission dictated by excited-state photophysics. To generate radiative excitons, the annihilation pathway was the first commonly-recognized ECL mechanism, where radical cations ($A^+$) and anions ($B^-$) are both generated at the same electrode by alternating potentials (AC) and recombine to form excited states (excitons A*, B* or exciplex/excimer AB*) before radicals are quenched, as shown in eq.1-3:[5, 6]

$$A - e \rightarrow A^+ \quad (1)$$

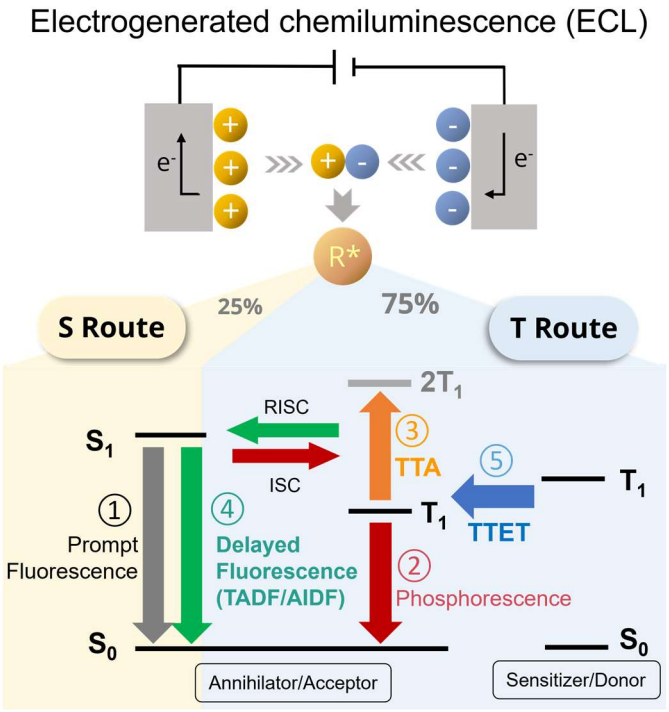
$$B + e \rightarrow B^- \quad (2)$$

(A=B, self-annihilation; A≠B, mixed annihilation)

$$A^+ + B^- \rightarrow A^* + B \; or \; B^* + A \; (or \; AB^*) \quad (3)$$

$$A^*(or \; B^*, \; AB^*) \rightarrow A \; (or \; B, AB) + h\nu \quad (4)$$

Due to the advantages of direct electron transfer and high-purity exciton generation, annihilation ECL has been abundantly studied in the fundamental research and material science, and played a crucial role in the early development of ECL theory. However, non-aqueous or aprotic solvents are normally required to stabilize radical ions before recombination, which has historically limited the practical application of annihilation-type ECL. This challenge motivated the development of coreactant ECL since the 1980s, where a coreactant is introduced alongside the luminophore to overcome the solvent limitations.[7-10] In coreactant ECL, both the luminophore and the coreactant undergo electrochemical reactions at a single applied potential, either anodic or cathodic. The resulting coreactant-derived radicals then react with the luminophore radicals to produce excitons. The relatively high stability of these coreactant radicals in aqueous media enables efficient ECL emission in water, greatly enhancing the versatility and applicability of this approach. The evolution from annihilation to coreactant ECL has significantly expanded ECL's impact, particularly in biosensing and medical diagnostics, where stable and efficient luminescence is essential. Some notable examples include the introduction of luminol/peroxide and $Ru(bpy)_3^{2+}$/TPrA (tripropylamine) systems, which revolutionized clinical and medical diagnostics, particularly with the commercialization of Roche's ECL-based immunoassay platform.[11-17]




**Scheme 1** The schematic illustration of annihilation ECL generation and the photophysical mechanisms and kinetic processes involved.

The ECL quantum efficiency ($\Phi_{\mathrm{ECL}}$) quantifies the overall performance of an ECL system and can be described as a product of several key contributing factors, as outlined below:[18]

$$\Phi_{\mathrm{ECL}} = \frac{\nu_{pho}}{\nu_{electron}} \times 100\% = \Phi_{\mathrm{exc}} \times \Phi_{\mathrm{S/T}} \times \Phi_{\mathrm{PL}} \times \Phi_{\mathrm{out}} \quad (5)$$

where $\nu_{phot}$ and $\nu_{electron}$ represents the number of electrons injected and photons emitted; $\Phi_{\mathrm{exc}}$ is the efficiency of exciton formation per injected electron, $\Phi_{\mathrm{S/T}}$ denotes the fraction of radiative excitons including singlets (S) and triplets (T) determined by spin statistics, and $\Phi_{\mathrm{PL}}$ is the photoluminescence (PL) quantum yield of the luminophore and $\Phi_{\mathrm{out}}$ corresponds to the light out-coupling efficiency. Therefore, beyond the efficiency of exciton generation through radical anion–cation recombination, $\Phi_{\mathrm{ECL}}$ also depends on $\Phi_{\mathrm{S/T}}$ of the resulting excitons. Unlike photoluminescence, which is governed by optical spin selection rules and thus favors singlet-state formation, exciton generation in ECL follows spin statistics, yielding an ideal 1:3 ratio of singlet to triplet states, as illustrated in Scheme 1. Depending on the spin state of generated excitons, ECL processes are generally classified into 'S route' (eq. 6) and 'T route' (eq. 7). The S route requires that the enthalpy of the electron-transfer reaction exceeds the energy of the emitter's lowest excited singlet state ($S_1$), i.e. in an 'energy sufficient' ECL system; otherwise for energy-deficient systems, the T route may prevail, wherein the lowest excited triplet state ($T_1$) is formed directly.

$$A^- + B^+ \rightarrow {}^1A^* + B \; or \; {}^1B^* + A \quad (6)$$

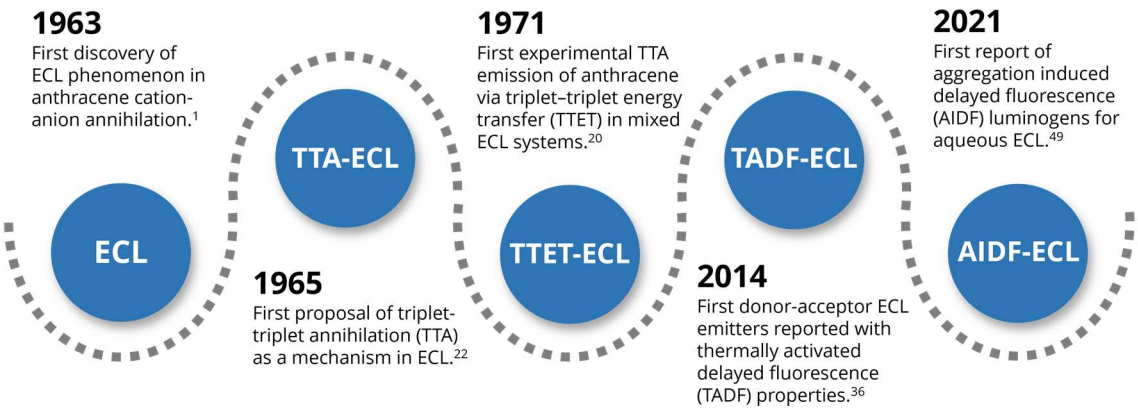
$$A^- + B^+ \rightarrow {}^3A^* + B \; or \; {}^3B^* + A \quad (7)$$

T route has been commonly employed to populate triplet states or to estimate the triplet energy by mixed annihilation with selected cation or anion radicals, depending on their redox potentials.[19, 20] Compared to the S route, which generates 25% singlet excitons that rapidly decay via prompt fluorescence, the T route yields up to 75% long-lived triplet excitons. Leveraging these triplets in ECL systems significantly enhances quantum efficiency. Due to spin conservation rules, the direct transition from

triplet excitons to the ground singlet state ($S_0$) is spin-forbidden, leading to slow radiative decay as weak phosphorescence. If systems exhibit weak spin-orbit coupling (SOC), a quantum mechanical parameter illustrating how an electron's spin interacts with its orbital angular momentum, the triplets may instead relax through non-radiative pathways, dissipating energy as heat. However, the fate of the 75% triplet states could be rewritten by manipulating two factors: 1) SOC and 2) the energy gap ($\Delta E_{ST}$) between the singlet and triplet states. High SOC promotes the mixing of singlet and triplet wave functions leading to perturbations in energy levels and rendering previously spin-forbidden transitions partially allowed. Incorporating heavy metal atoms such as iridium, platinum, or ruthenium into metal complex luminophores is a common strategy to enhance SOC, thereby promoting both radiative decay from triplet states and efficient singlet-to-triplet transitions via allowed intersystem crossing (ISC). This facilitates nearly 100% population of emissive triplet states, leading to enhanced phosphorescence. The model phosphorescent luminophore, $Ru(bpy)_3^{2+}$ complex, which exhibits relatively short radiative lifetime (~600 ns) in aqueous solution and ~5% absolute $\Phi_{ECL}$ (at a rotating disk-ring electrode) is relatively highly luminescent from triplet metal-to-ligand charge transfer excited states ($^3$MLCT), has been widely employed in ECL studies and applications since discovered in 1972.[21]

Conversely, dark triplet excitons can be upconverted to singlet excitons via reverse intersystem crossing (RISC), leading to delayed fluorescence (DF) and potentially boosting $\Phi_{S/T}$ to 100% before non-radiative decay or quenching occurs. Achieving efficient RISC requires a small $\Delta E_{ST}$ and strong SOC, both of which can be tuned through molecular design of the luminophore. Additionally, the relatively long lifetime of triplet excitons enhances the overall stability of the luminescence signal and allows for a greater probability of spin transition or energy transfer (ET), increasing the efficiency of light emission. Further, triplet states are more energetically favourable due to unpaired spin configuration and thus less electron-electron repulsion. Therefore, compared to direct activation of singlet states by a higher applied voltage, the overall turn-on voltage and power consumption can be realized by triplet-to-singlet conversion via triplet fusion or thermal-induced RISC. Owing to the paramagnetic nature of triplet excitons, magnetic field effects (MFEs) can be leveraged to enhance the emission intensity in triplet-involved ECL systems, either by modulating the singlet-to-triplet population ratio in the emissive states or by suppressing triplet quenching caused by paramagnetic radical ions. Overall, by manipulating these spin-dependent processes, the excited-state dynamics can be tailored to maximize light emission and lower power consumption.

In this review, we explore the role of triplet dynamics in the advancement of ECL research. Instead of focus on singlet-to-triplet conversion, as widely employed in heavy-metal phosphorescent ECL, this review emphasizes T-route ECL pathways that utilize triplet-to-singlet upconversion mechanisms, including the well-established triplet–triplet annihilation (TTA) and the emerging strategies of thermally activated delayed fluorescence (TADF) and aggregation-induced delayed fluorescence (AIDF). These mechanisms intrinsically enhance the $\Phi_{S/T}$ from 25% to 62.5% and 100%, respectively. To address the inherent limitations of ECL luminophores in triplet generation, we also review the strategies relying on triplet-to-triplet energy transfer (TTET) via selected triplet donors or sensitizers. Furthermore, we summarize key characterization methods and theoretical approaches for distinguishing these mechanisms from direct singlet formation. Representative materials developed along the trajectory of ECL research are highlighted from a structure-function perspective. While both intrinsic and extrinsic challenges remain in leveraging triplet states for efficient ECL, their integration significantly enhances the potential of ECL materials and techniques, paving the way for brighter application prospects.




**Scheme 2** The timeline of key developments in triplet-involved ECL mechanisms.

# 2. Triplet-Involved Mechanisms in ECL

Advancements in understanding and controlling the dynamics of triplet states in light emission processes are crucial for fully utilizing triplet states for high ECL efficiency. In the following sections, we review the previously reported triplet-involved ECL mechanisms, as shown in Scheme 1, including triplet-to-singlet conversion strategies, e.g. TTA, TADF, AIDF and TTET that enhances triplet population. Scheme 2 summarizes the historical evolution of ECL techniques, classified according to their underlying mechanistic pathways. Despite six decades of progress, fully harnessing the advantages of triplet states in ECL remains challenging. A deeper understanding and clear demonstration of these mechanisms are essential for advancing next-generation ECL systems with enhanced performance.

### 2.1 Triplet-triplet annihilation (TTA)

Since G. J. Hoijtink first proposed triplet–triplet annihilation as a potential ECL pathway in 1965,[22] early studies on annihilation ECL have centered around a key question: whether the emission originates directly from singlet excited states or via a TTA pathway. Unlike the singlet-route, the TTA-ECL mechanism involves the electrochemical generation of two triplet excitons, which subsequently undergo annihilation to form a singlet exciton (eq. 8), followed by fluorescence emission.

$$^3A^* + {}^3A^* \rightarrow {}^1A^* + A \quad (8)$$

Efficient TTA must be both energetically and kinetically favoured. The singlet energy of the annihilator should be lower than twice its triplet energy ($2T_1 > S_1$) to enable efficient upconversion. Fully meeting these requirements, hydrocarbons such as rubrene, anthracene, and 9,10-dimethylanthracene (DMA) were demonstrated in early ECL studies emitting via TTA followed by cation–anion recombination in selected aprotic solvents.[23-25] Additionally, a high triplet population is essential to increase the probability of triplet-triplet encounters. To achieve that, establishing energy-deficient systems for direct electrochemical triplet generation, along with employing efficient triplet sensitizers or donors and optimizing working conditions to promote exciton migration while minimizing self-quenching and oxygen quenching, are essential considerations.

The first experimental evidence of TTA in ECL was reported in 1968 by Chang et al., based on rubrene in benzonitrile.[24] Non-emissive easily-reduced p-benzoquinone or easily-oxidized *N,N,N',N'*-tetramethyl-*p*-phenylenediamine (TMPDA) or *p*-phenylenediamine (PPDA) were incorporated respectively as electron donor/acceptor for rubrene cation/anion radicals to produce rubrene triplets in energy-deficient anion-cation annihilation, which eventually generates fluorescence via TTA on rubrene. Since then, a growing

number of energy-deficient aromatic hydrocarbon/organic donor–acceptor radical pairs have demonstrated T-route and TTA-based ECL behaviour in mixed systems. These include anthracene, 9,10-diphenylanthracene (DPA), rubrene, and fluoranthene anions with *N,N*-dimethyl-*p*-phenylenediamine; 10-methylphenothiazine[19] or benzoyl peroxide (BPO) cations as electron acceptor;[26] anthracene anions with 4,N,N-trimethylaniline (TMA) cations;[27] perylene anions or cations with tri-p-tolylamine (TPTA) cations or benzil anions respectively;[28] tetraphenylpyrrole (TPP) or tetraphenylthiophene (TPT) cations with naphthalene anions;[29] and thianthrene (TH) cations with 2,5-diphenyl-1,3,4-oxadiazole (PPD) anions.[30] Wightman's group reported the efficiency of photon production at high concentrations of DPA by the T-route (0.012) approached that of the S-route, and is much higher than previously reported, suggesting that it may be an alternate scheme to employ in solid-state display devices.[31] They also utilised a series of triarylamine hole-transport materials to cross-react with derivatives of aluminum quinolate and quinacridones, which were of interest in organic light-emitting diodes (OLED), to generate ECL through TTA pathways with the maximum efficiency of several percent. The TTA route was confirmed by the second-order reaction kinetics and the shape of ECL-time response.[32] Elangovan et al proposed two types of emitters, including arylethynylacridines and donor-substituted phenylethynylcoumarins, which follow TTA route for ECL due to energy insufficiency in self-annihilation by comparing the annihilation enthalpy change values with the ECL maxima.[33, 34] Ishimatsu et al reported TTA-ECL of a borondipyrromethane (BODIPY) derivative due to energy insufficiency while it changes to direct singlet formation within a coreactant system.[35]

### 2.2 Thermally activated delayed fluorescence (TADF)

Since 2014, the foundational work by Ishimatsu et al. has opened new avenues for enhancing ECL through TADF in purely organic systems.[36] It offers a pathway to overcome spin statistical limitations, enabling up to 100% exciton utilization through efficient RISC:

$$^3A^* \xrightarrow{RISC} {}^1A^* \tag{9}$$

Two key parameters, $\Delta E_{ST}$ and SOC, are critical to the RISC rate and TADF efficiency. A small $\Delta E_{ST}$, typically around or below 0.3 eV,[37] facilitates RISC by allowing thermal upconversion from the triplet to the singlet excited state. This process can be quantitatively described by Fermi's Golden Rule (eq. 10).[38] Additionally, the Franck–Condon weighted density (FCWD), as defined in eq. 11 based on Boltzmann statistics, quantifies the vibrational overlap between the initial triplet and final singlet electronic states. At finite temperatures, this overlap can be approximated as a thermally activated process. Consequently, a small $\Delta \mathrm{E_{ST}}$ ensures RISC can occur with ambient thermal energy, while sufficient SOC facilitates the required spin transitions. Thus, optimal TADF performance demands a fine balance: minimised $\Delta E_{ST}$, enhanced SOC, and molecular rigidity to suppress non-radiative decay.

$$k_{RISC} = \frac{2\pi}{\hbar}|V_{SOC}|^2 FCWD \approx A\exp\left(-\frac{\Delta E_{ST}}{k_B T}\right) \tag{10}$$

$$FCWD(E) = \sum_{n,m}\frac{e^{-\beta E_{T,n}}}{Z}\left|\langle\psi_{vib}^{S,m}(Q)|\psi_{vib}^{T,n}(Q)\rangle\right|^2 \delta\left(E - E_{S,m} + E_{T,n}\right) \tag{11}$$

Based on this consideration, Ishimatsu et al. designed donor–acceptor (D–A) type TADF molecules for ECL systems, relying on their significant spatial separation between the highest occupied molecular orbital (HOMO) and the lowest unoccupied molecular orbital (LUMO) that reduces the overlap and decreasing $\Delta E_{ST}$. This design enables efficient RISC under ambient conditions, enhancing luminescence efficiency. Ishimatsu's approach demonstrated that TADF-based ECL systems could achieve efficiencies significantly higher than traditional fluorescent ECL molecules, with certain TADF molecules 4CzIPN reaching approximately 50% $\Phi_{\mathrm{ECL}}$ in dichloromethane.

However, working with triplet states introduces significant challenges, particularly the quenching effects of molecular oxygen on triplet excitons, which can substantially limit ECL efficiency.[39] To address this issue, strategies involving polymers and nanoparticles, such as quantum dots, have been developed to encapsulate TADF molecules.[40, 41] These encapsulating materials serve as barriers against oxygen quenching, enabling efficient triplet harvesting even in oxygen-rich environments. This approach not only enhances the stability of the TADF materials but also improves their processability for practical applications. In this regard, the development of polymer-based systems marks a noteworthy advancement. Later advancements in the field have focused on optimising molecular design to enhance triplet state dynamics. Precise control over $\Delta E_{ST}$ is essential: if the gap is too large, RISC becomes inefficient; if too small, non-radiative decay or excimer formation may dominate, diminishing ECL performance.

### 2.3 Aggregation-induced delayed fluorescence (AIDF)

Since the pioneering report by De Cola's group in 2017 on the supramolecular assemblies of square-planar Pt(II) complexes via Pt···Pt interactions, aggregation-induced electrochemiluminescence (AIECL) has garnered significant attention.[42-48] Despite this, achieving high efficiency remains a considerable challenge. To address this, more recent strategies have combined TADF with aggregation-induced emission (AIE), giving rise to aggregation-induced delayed fluorescence (AIDF) luminogens for ECL applications. In aggregated states, AIE helps reduce $\Delta E_{ST}$ facilitating triplet-to-singlet spin upconversion characteristic of TADF by restricting non-radiative molecular motions.

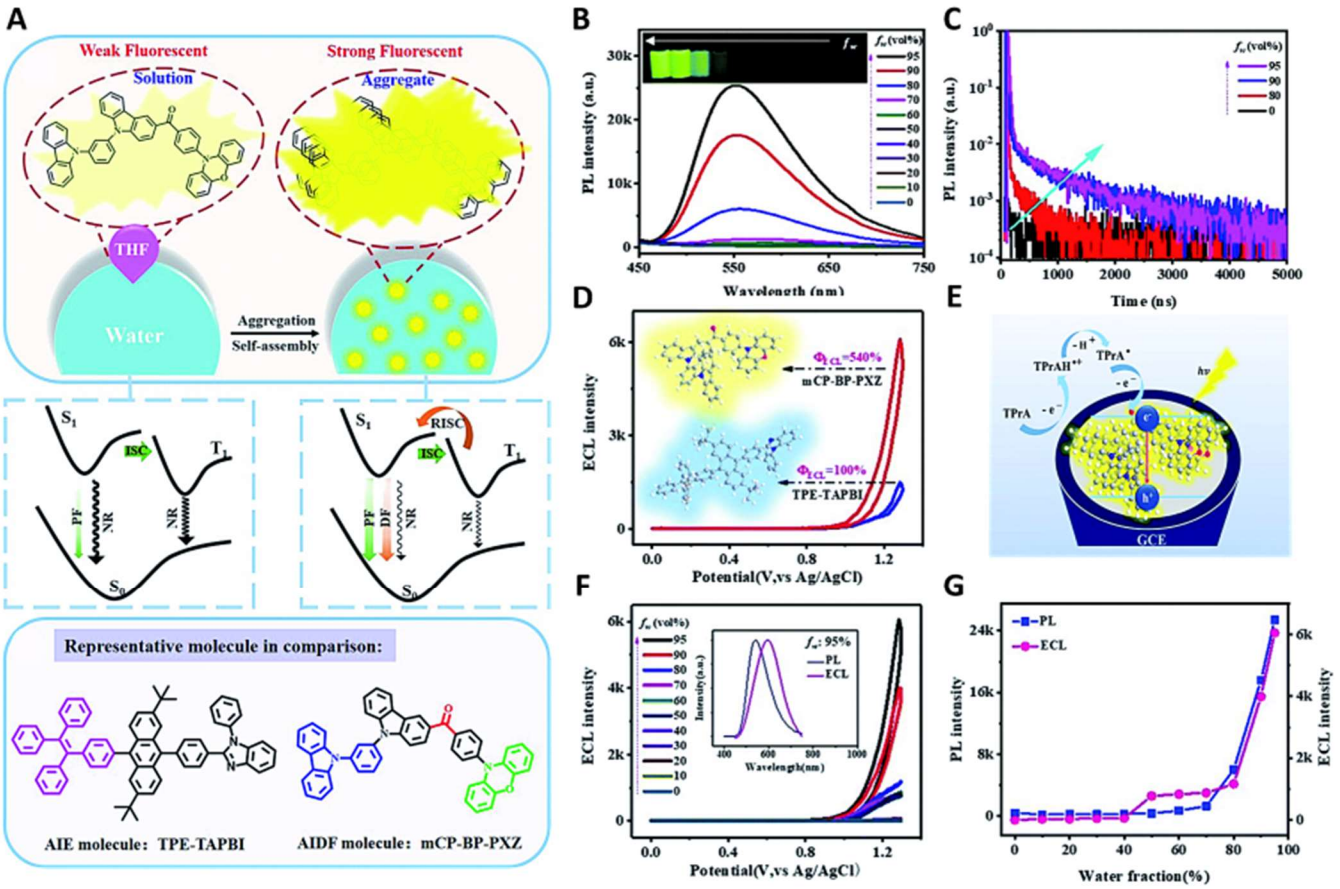



**Fig. 1** (A) Preparation of AIDF luminogens via self-assembly in mixed solvent, with photophysical transitions shown in solution and aggregated states. (B) PL spectra and (C) transient PL decay curves of mCP-BP-PXZ with different

water fractions ($f_w$) in THF/water mixed solutions. (D) The oxidative-reduction ECL responses for the AIDF and AIE molecules at $f_w$=95%. (E) The schematic oxidative-reduction ECL processes, (F) ECL curves and (G) ECL intensities of the AIDF-luminogen-modified GCE/TPrA system in a range of $f_w$. Reproduced with permission from ref. 49. Copyright 2021 Royal Society of Chemistry.

AIDF luminogens—extensively developed for organic light-emitting diodes (OLEDs)—have only recently found successful application in ECL systems. Notably, in 2021, a purely organic AIDF luminogen, mCP-BP-PXZ, was first applied in an aqueous co-reactant ECL system. Owing to its enhanced RISC kinetics, which is enabled by reduced $\Delta E_{ST}$ (0.024 eV), improved spin–orbit coupling (SOC) and suppression of non-radiative decay from $S_1$ to $S_0$ in the aggregated state (Fig. 1A–C), the system achieved a 5.4-fold increase in relative $\Phi_{ECL}$ compared to a tetraphenylethylene (TPE)-based AIE reference lacking delayed fluorescence properties (Fig. 1D).[49] The consistency between PL and ECL intensity on the increasing trend with the fraction ($f_w$) of poor solvent (e.g. $H_2O$) for mCP-BP-PXZ-modified GCE electrodes (Fig. 1E-G) was claimed characteristic for the AIDF-ECL mechanism. For delayed ECL, the quantum efficiency ratio between ECL and PL, as so-called K value,[50] represents the distribution of delayed fluorescence by RISC or triplet states to the enhanced ECL. Gao et al. constructed organic dots (OD) within a donor-acceptor (D-A) structure and achieved 12-fold and higher K values in comparison with AIE-active-only analogues containing an extra phenyl ring in between. The high twisted conformation observed in the single crystal was considered responsible for the HOMO/LUMO separation thus reducing $\Delta E_{ST}$ to 0.013 eV and also no apparent $\pi$-$\pi$ interactions in a rigidified molecular packing by abundant hydrogen bonds. Introducing dual D-A pair in the rational design further promotes the RISC efficiency by involving triplets both at $T_1$ and $T_2$, while tuning the D-A relative position regulates the SOC of these low-lying excited states, such as x($S_1$, $T_1$), x($S_1$, $T_2$), which also determines the effective RISC pathway. Alternatively, introducing a *tert*-butoxy group into the acceptor endows the molecule with further restriction and accelerates the radiative decay, showing 2-fold higher ECL efficiency.[51]

### 2.4 Triplet-to-triplet energy transfer (TTET)

Despite significant progress, the availability of materials that fully satisfy the essential criteria for efficient ECL luminophores—namely, reversible electrochemical behaviour, stable radical intermediates, and outstanding optical and photophysical properties—remains limited. One promising strategy to overcome this limitation involves integrating an electroactive exciton donor, capable of generating long-lived excitons (such as triplet states), with an inert, high-quantum-efficiency luminophore that serves as the exciton acceptor. This donor–acceptor pairing could expand the design landscape for efficient ECL systems relying on efficient energy transfer. While numerous energy transfer chemiluminescence (CL) systems have been developed for the detection of fluorophores,[52-55] energy-transfer ECL offers distinct advantages for advanced analytical and sensing applications.

A common case involves utilizing triplet sensitizers to populate the triplet exciton pool electrochemically for the subsequent use in TTA, DF or phosphorescence pathways via TTET. This approach not only enhances ECL efficiency but also lowers the required driving potential and improves operational stability. To enable efficient TTET in an ECL system, the triplet energy level of the donor must be higher (~0.2 eV) than that of the acceptor to allow efficient and diffusion-controlled energy transfer.[19, 20, 56] Additionally, the acceptor should remain electroinactive within the potential window of interest to generate the donor species, and chemically inert towards the generated radical ions.

Benzophenone is a favourable organic triplet ECL emitter characterized by a very small $\Delta E_{ST}$ and an ISC yield approaching unity. Owing to its high triplet production efficiency, it has been employed to sensitize TTA of naphthalene in ECL systems.[57] The triplet energy level of benzophenone is approximately

0.4 eV higher than that of naphthalene, enabling efficient TTET between the two (TTET efficiency ≈ 0.75). Importantly, the redox potential of naphthalene lies well outside the range required for mixed annihilation processes that would otherwise generate benzophenone triplets. As a result, this donor–acceptor pair gives rise to a new ECL emission at 330 nm, corresponding to the singlet-excited state of naphthalene, along with partially quenched phosphorescence from benzophenone at 437 nm. Heavy-metal complexes such as $Ru(bpy)_3^{2+}$, has been also employed as a triplet sensitizer doping into DPA wires or DPA-containing light-emitting device.[58, 59] $Ru(bpy)_3^{2+}$ exhibits significantly lower positive oxidation potential (~1.1 V *vs* Ag/AgCl) than DPA (~1.5V) but possesses higher triplet energy (~2.03 eV *vs* ~1.77 eV for DPA). Therefore, under a lower potential, emissive $Ru(bpy)_3^{2+}$ triplets generated either via TPrA-mediated anodic reactions[58] or under AC bias,[59] functions as an donor transferring energy to DPA as an annihilator in the subsequent TTA process (schematically illustrated in Fig. 2A), generating a blue upconverted emission. The trade-off between red (~620 nm) and blue (~440 nm) ECL (as separately shown in Fig. 2B), which can be modulated by adjusting either the molar ratio of the two components (Fig. 2C)[58] or the applied potential (Fig. 2D),[59] reflects two distinct emissive pathways that share a common intermediate ($Ru(bpy)_3^{2+}$ triplets) and rely on the efficient TTET. Building on this mechanism, an ultrafast-response (<100 μs) blue ECL from DPA was achieved by exploiting the rapid electrochemical response of the $Ru(bpy)_3^{2+}$ and subsequent TTET to DPA within a DNA-modified mesoscopic electrode structure.[60] This DNA/ $Ru(bpy)_3^{2+}$- DPA hybrid design successfully reduced the required AC potential to 2.2 V and extended the upper frequency limit to over 10 kHz (Fig. 2E), thereby significantly improving operational lifetime.

Sulfite has been also employed as an energy transfer mediator in ECL analysis due to its ability to produce triplet-state sulfur dioxide ($^3SO_2$*) under electrochemical oxidation. Although $^3SO_2$* emits weakly, it efficiently transfers energy to highly emissive and functional fluorophores, such as rhodamine B[61] and $Tb^{3+}$–ligand system, where ligands include Norfloxacin (NFLX), tosufloxacin (TFLX),[62, 63] pipemidic acid (PPA)[64] etc. In the $Tb^{3+}$–ligand–$Na_2SO_3$ ECL system, the observed emission originates from the excited $Tb^{3+}$ state ($^5D_4$), which is believed to result from a two-step energy transfer process: first, an intermolecular transfer from $^3SO_2$* to the ligand, followed by an intramolecular transfer from the ligand to the central $Tb^{3+}$ ion in the chelate complex. This ECL approach, utilizing $Na_2SO_3$ as a sensitizer and $Tb^{3+}$ as the luminophore, offers a robust platform for ligand analyte detection, characterized by a wide linear range and low detection limits, and demonstrates significant potential for applications in clinical diagnostics.

Recent studies have increasingly leveraged the intramolecular energy transfer mechanism—commonly known as the "antenna effect"—in lanthanide metal–organic frameworks (LMOFs) to enhance ECL performance, particularly for biosensing applications. In these systems, organic linkers act as efficient antennas that harvest energy and transfer it to the lanthanide centre, thereby overcoming the Laporte-forbidden nature of *f–f* transitions.[65-67] For effective energy transfer, the lowest triplet energy level of the antenna ligand must closely match or slightly exceed the resonance energy of the lanthanide ion. Consequently, the rational selection and design of organic ligands with appropriately tuned triplet energy levels are critical to maximizing forward energy transfer and minimizing back-transfer losses.[68] Wang et al. developed europium-based MOFs employing 5-boronoisophthalic acid as the antenna ligand, enabling efficient energy transfer to $Eu^{3+}$ and yielding strong self-luminescence with high ECL sensitivity in immunoassay.[69] More recently, Dong et al. introduced a mixed-ligand strategy to further enhance ECL output, as shown in Fig. 2F-I, utilising a primary antenna ligand (e.g., $NH_2$–$H_2BDC$) and an auxiliary ligand (e.g., 1,10-phenanthroline). This synergistic approach fine-tunes the energy gap between the triplet ligand and the excited state of $Eu^{3+}$ while suppressing nonradiative losses. The mixed-ligand design not only increases the number of viable energy-transfer channels (Fig. 2G) but also lowers the excitation potential, effectively addressing the challenge of biocompatibility in ECL-based biosensing systems.[70]

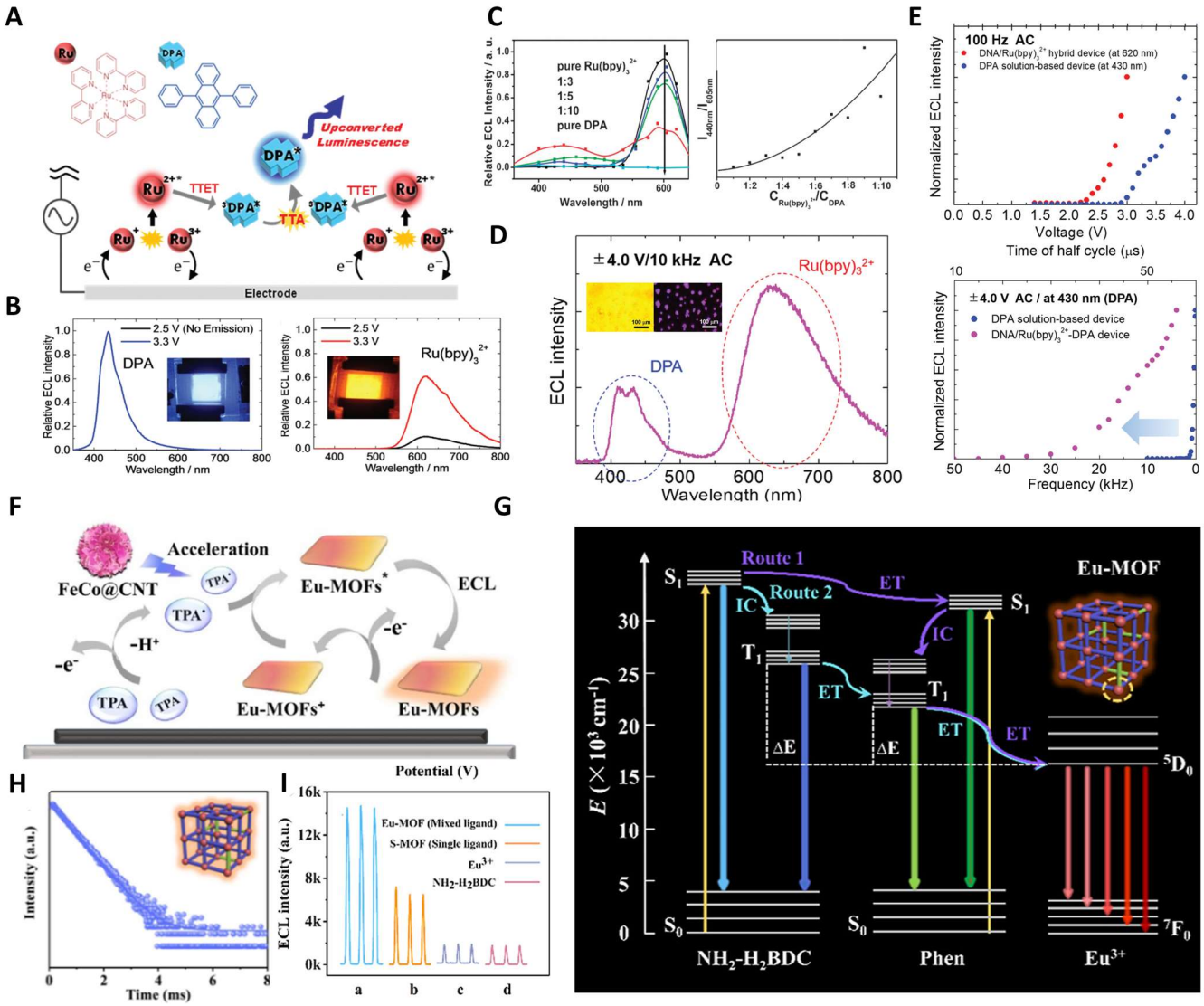



**Fig. 2** (A) Schematic illustration of the emission mechanism of the $Ru(bpy)_3^{2+}$/DPA mixed solution. (B) ECL spectra of DPA or $Ru(bpy)_3^{2+}$-only solutions. (C) ECL spectra (left) and the ECL intensity ratios of DPA (440 nm) to $Ru(bpy)_3^{2+}$ (605 nm) as a function of the molar ratio in the doped wires. (D) ECL spectra of the DNA/$Ru(bpy)_3^{2+}$–DPA hybrid device under AC conditions. Inset: fluorescence microscopic image of DNA/$Ru(bpy)_3^{2+}$–DPA system. (E) Voltage dependence and frequency dependence of ECL intensity from the DNA/$Ru(bpy)_3^{2+}$–DPA hybrid device and DPA solution-based device. (F) Co-reactant ECL processes of the Eu-MOF-TPrA system. (H) PL decay curves of the Eu-MOF. (I) ECL performance of various luminophores. (G) Schematic illustration of triplet-triplet energy-transfer routes from mixed ligands to $Eu^{3+}$ centre in the Eu-MOF. (A)-(B) Reproduced with permission from ref. 60. Copyright 2019 Royal Society of Chemistry. (C) Reproduced with permission from ref. 58. Copyright 2012 Royal Society of Chemistry. (D)-(E) Reproduced with permission from ref. 59. Copyright 2021 Royal Society of Chemistry. (F)-(I) Reproduced with permission from ref. 70. Copyright 2022 American Chemical Society.

# 3. Triplet-Probing Methods and Theories

Given the critical influence that triplet excitons may exert on ECL intensity, stability, and emission dynamics, a deeper understanding of their involvement is essential. Nowadays, a commonly employed approach to probe the ECL mechanism is by comparing the fluorescence and ECL emission spectra. A good spectral match typically suggests that the emission arises from the singlet excited state of the

luminophore. However, such comparisons are insufficient to confirm or rule out the participation of triplet states in the ECL process. In this section, we summarize the key methodologies that have been used to detect and verify the presence of triplet states in ECL mechanisms. These methods and theories are categorised and discussed from the perspectives of thermodynamic characteristics, kinetic behaviours, and magnetic field effect. By highlighting both the strengths and limits of each approach, we aim to provide a comprehensive overview and offer insights for more accurate mechanistic elucidation and future luminophore design.

### 3.1 Thermodynamic Evidence for Triplet Involvement in ECL

**3.1.1 Energy sufficiency.** In annihilation-based ECL, efficient light emission requires the electron-transfer enthalpy between electrochemically generated species to be sufficient to directly populate the excited state responsible for luminescence. Traditionally, this energy sufficiency is evaluated with respect to the singlet excited state, assuming that the emitting state is formed directly from the annihilation reaction. To visualise this, researchers have plotted the fluorescence emission wavelength ($\lambda_{em}$) against the electrochemical gap ($\Delta E_{1/2}$), defined as the potential difference between the oxidation and reduction peaks ($E_{1/2}^{ox}$-$E_{1/2}^{red}$) obtained via cyclic voltammetry. This plot creates a so-called "energy sufficiency wall", as shown in Fig. 3, which provides a quantitative framework for estimating the minimum redox gap required to generate ECL at a given emission wavelength.[71] This approach enables rapid screening of luminophores for their ECL feasibility based on thermodynamic criteria.

However, in systems where the overall reaction enthalpy is insufficient to populate the singlet excited state but still exceeds the energy of the triplet state, the initial excitation may form a triplet instead. These triplets can subsequently undergo TTA to yield an emissive singlet state. To experimentally demonstrate this, a concept known as the "critical enthalpy" has been introduced. By conducting ECL experiments with various co-reactant radicals of known redox enthalpies and observing the threshold energy at which luminescence begins, one can estimate the minimum enthalpy required for emission. If this critical value aligns with the energy of the lowest triplet state rather than the singlet, it provides strong evidence that triplet intermediates play a key role in the luminescence process.[19]

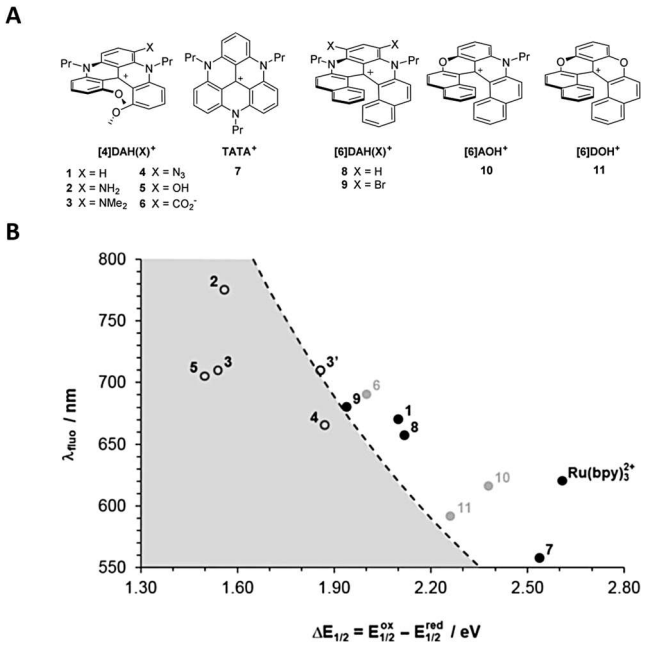


**Fig. 3** (A) Chemical structures and (B) ECL wall of energy sufficiency of cationic helicenes and helicenes in the annihilation mode, indicating the redox potential gap threshold required for a luminophore to emit for a given wavelength. Reproduced with permission from ref. 71. Copyright 2017 Wiley-VCH.

**3.1.2 Chemically inert triplet quenchers.** In the early stages, a range of chemically inert yet triplet-active quenchers have been employed to probe the involvement of triplet intermediates in ECL emission. These quenchers possess triplet energy levels lower than those of the emitter, enabling efficient non-radiative energy transfer. Additionally, their redox potentials lie well outside the applied electrochemical window, ensuring minimal interference with the redox processes of the system.

$$3A^{*} + \ trans - \text{stilbene} \rightarrow A + \ cis - \text{stilbene} \tag{12}$$

Zweig et al. investigated phenanthrene-based ECL in the presence of triplet quenchers such as 1,3,5-hexatriene and 2,3-dimethylbutadiene, demonstrating that the green emission arises from phosphorescence of the phenanthrene triplet state.[72] Later, Freed and Faulkner examined the ECL mechanism of the fluoranthene/10-methylphenothiazine (10-MP) system using *trans*-stilbene, anthracene, and pyrene as triplet quenchers. With triplet energies ~0.3–0.5 eV below that of fluoranthene, these quenchers modulated the emission behaviour differently: *trans*-stilbene suppressed luminescence via *trans*-to-*cis* isomerization (eq. 12), while anthracene and pyrene produced strong blue-violet emission instead via sensitized TTA.[19] These findings confirmed the formation of a fluoranthene triplet intermediate and supported a triplet-mediated (T-route) ECL pathway under energy-deficient conditions. Additionally, trans-stilbene was used to estimate triplet yields, initially as low as 0.7%, but approaching unity in the fluoranthene/10-phenylphenothiazine (10-PP) system when accounting for isomerization efficiency.[20, 73]

### 3.2 Kinetic Indicators of Triplet State Participation

**3.2.1 Time-resolved ECL under controlled potential.** Distinguishing between TTA and direct singlet formation in ECL solely by comparing ECL and PL spectra can be challenging due to their often-similar emission profiles. To address this, Feldberg introduced a theoretical framework in 1966 that analyses the kinetics of ECL under controlled potential conditions, particularly using a double-potential step method.[74-76] In this approach, a sufficiently positive potential is applied during the forward step (duration $t_f$) to oxidize the emissive species into cation radicals instantaneously. Subsequently, a negative potential is applied during the reverse step (duration $t_r$) to generate radical anions, as exemplified in Fig. 4A. These oppositely charged radicals diffuse and annihilate within the diffusion layer, forming excited states that emit light.

Feldberg's model quantitatively examines the ECL intensity-time decay curves resulting from these processes. In this model, the ECL intensity-time correlation (Fig. 4B) in the second/light emitting step could be linearised as follows,

$$logP = a_i + b_i(t_r/t_f)^{1/2} \tag{13}$$

Here, $P$ represents the photomultiplier current, $t_f$ is the duration of the forward potential step (oxidation), $t_r$ is the duration of the reverse potential step (reduction), $a_i$ is an intercept constant, and $b_i$ is the slope associated with the specific emission pathway. The slope $b_i$ serves as a diagnostic indicator: a slope of approximately –1.45 suggests direct singlet formation and -2.9 indicates excited singlet formation via TTA.[77] These values are derived under the assumptions of stable reactants and significant triplet quenching by added triplet quenchers. Feldberg's pioneering work established the foundation for analysing ECL decay curves. By quantifying changes in the slope of the linearised "Feldberg plots", researchers can differentiate between the underlying emission mechanisms.

Chang et al observed the strong dependence of the slope $b_i$ on the forward step time ($t_f$) for rubrene cation-anion annihilation ECL system (Fig. 4C). As $t_f$ was reduced to below 1 s—under conditions where triplet quenching became significant—the slope increased to an average of –2.8. According to Feldberg's theories, this value suggests the involvement of rubrene triplets in the emission process.[24] Grabner et al also applied intensity–time analysis to energy-deficient annihilation systems such as perylene/tri-p-tolylamine and perylene/benzil. Their results supported the triplet-mediated ECL mechanism and were complemented by considerations of radical ion stability and the origin of triplet quenching.[28] Further advancing Feldberg's analysis, Bezman and Faulkner developed an extended model for triple-potential-step ECL generation. Besides the same forward and reverse potential steps, the third step returns to the rest potential to regenerate the initial starting conditions and avoid the reactant built-up. They introduced a concise set of quantum parameters, including an efficiency factor ($\alpha$) and a newly defined T-route quenching parameter ($\beta$), enabling experimental access to both the absolute $\Phi_{ECL}$ and the triplet formation efficiency ($\Phi_T$).[78] Calculations based on this extended model for the rubrene ECL system not only suggested that rubrene triplets were directly generated in the redox reaction and that the emitting singlet arises from triplet-triplet annihilation, but also estimated a triplet formation yield of 10–30%, with 50–100% of those triplets participating in the annihilation process.[79]

This decay-curve analysis provides a more definitive method for distinguishing between TTA and direct singlet formation pathways in ECL, beyond spectral comparisons. However, this analysis has its limitations, as the temporal profile can also be affected by side reactions, the time constant of the electrochemical cell, and uncompensated solution resistance. To address this, Collinson et al applied high-frequency voltammetry (20-30 kHz) in this analysis to reduce time scale and access reaction kinetics approaching the diffusion-control limit, by using a microelectrode which reduces the effects from double-layer capacitance and ohmic drop.[80] Moreover, this decay analysis is most applicable to systems where luminescence arises exclusively from either S or T route. In energy-sufficient systems, where S, T and mixed route are all possible, the mechanistic study requires more evidence from other methods, such as the effect of magnetic field and the effect of the triplet quenchers on the ECL decay curves.

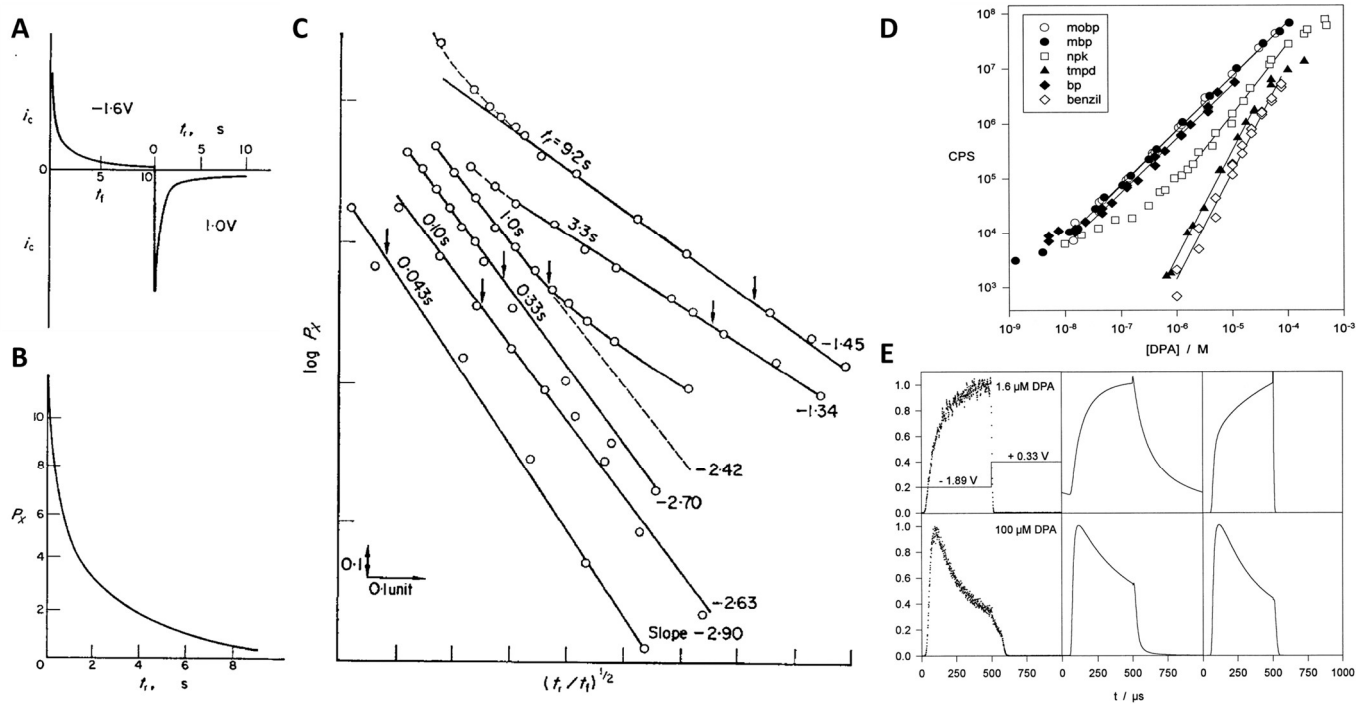


**Fig. 4** (A) Current/time curves of sequential reduction and oxidation of rubrene in benzonitrile. (B) Photomultiplier tube current, $P_x$ during time $t_r$. (C) Plots of log $P_x$ versus $(t_r/t_f)^{1/2}$ values as indicated. (D) Logarithmic plot of ECL intensity versus DPA concentration. (E) Normalized ECL (left panel) and simulated curves (centre and right panels) for DPA-containing energy deficient systems. (A)-(C) Reproduced with permission from ref.24. Copyright 1968 Elsevier B.V. (D)-(E) Reproduced with permission from ref.31. Copyright 1997 American Chemical Society.

**3.2.2 Reaction order.** Another kinetic approach to distinguishing ECL mechanisms—particularly in energy-sufficient systems—involves analysing the correlation between ECL intensity and the concentration of the limiting emitter, as demonstrated by Ritchie et al.[31] They investigated DPA-based ECL with various donors and acceptors, as depicted in Fig. 4D, using a flow-injection system that allowed for precise control and variation of reactant concentrations. To simplify mechanistic interpretation, they employed high-frequency ECL generation at microelectrodes, effectively minimising side reactions such as light quenching by impurities away from the electrode surface.

Using finite difference simulations that showed excellent agreement with experimental data (correlation coefficients > 0.999), they extracted distinct reaction orders for different emitter systems (Fig. 4D). These reaction orders aligned well with the thermodynamic feasibility of the respective ECL pathways. In energy-sufficient systems, a first-order dependence on emitter concentration (slope ≈ 1) indicated a singlet (S-route) mechanism. In contrast, energy-deficient systems exhibited second-order behaviour (slope ≈ 2), consistent with singlet formation via TTA, i.e., the T-route. Importantly, they also identified systems exhibiting intermediate reaction energies and mixed singlet–triplet behaviour, such as the $NPK^{\bullet-}$ /$DPA^{\bullet+}$ pair. In this intermediate case, the reaction order transitioned from one to two as the DPA concentration increased. A non-integer slope in this region suggested competing S- and T-route contributions. Beyond mechanistic assignments, their kinetic modelling (Fig. 4E) also provided estimates of relevant rate constants and revealed a high T-route efficiency (up to 24%) after correcting for quenching effects.

In a similar study, Gross et al. examined the reaction order and light emission time profiles for aluminum quinolate ($Al(qs)_3$) and quinacridone (DIQA) systems paired with different triarylamine donors.[32] By maintaining the triarylamine donors in excess, they analysed the dependence of ECL intensity on DIQA concentration. Logarithmic plots of light intensity versus DIQA concentration revealed distinct reaction orders for different donors: a slope of approximately 1 for ETBC indicated a S-route mechanism in an energy-sufficient system, while a slope near 2 for TPD suggested a TTA (T-route) mechanism consistent with energy-deficient conditions.

In addition to analysing emitter concentration dependence, the correlation between the ECL light emission rate *I* (einsteins/s) and the electron transfer rate *N* (mol/s) also serves as a mechanistic indicator. The correlation is described by:

$$I = \Phi_f \Phi_S N^n \tag{14}$$

where $\Phi_S$ is probability of singlet formation during radical-ion annihilation and $\Phi_f$ is the fluorescence efficiency. For S-route, the reaction order *n* exhibits unity due to a linear correlation between *I* and *N* as $\Phi_S$ and $\Phi_f$ are assumed constant for a given system. However, for the thianthrene (TH) ECL system using the 2,5-diphenyl-1,3,4-oxadiazole (PPD) as the donor, which had been previously classified as the S-route due to sufficient reaction energy to populate excited singlets ($^1TH^*$) and the absence of a magnetic field effect,[81] Michael and Faulkner reported a quadratic dependence of light intensity on redox reaction rate (*n*=2) by analysing the light and current transients in the triple-potential-step experiment.[30] Further evidences, including low chemiluminescence yield and strong sensitivity to pretreatment conditions, also supported its reassignment to a purely T-route mechanism.

### 3.3 Magnetic Field Effects in ECL Mechanism Studies

In addition to their distinct kinetic signatures, triplet states in ECL exhibit magnetic field effects (MFEs) due to their paramagnetic nature. These effects provide a powerful complementary tool for distinguishing between ECL mechanisms. All triplet-involved processes—including triplet generation (whether directly via electron transfer or indirectly via ISC or reverse ISC, triplet–triplet annihilation, and triplet–radical ion interactions—are sensitive to external magnetic fields. The rates of key triplet-based reactions, such as TTA or quenching by paramagnetic species (e.g., radical ions or molecular oxygen), can be modulated by the magnetic field strength and orientation.

The pioneering work by Johnson et al. on crystalline anthracene first demonstrated that the intensity of annihilation luminescence from triplet excitons varied with the applied magnetic field. The observed changes were attributed to field-induced modulation of the TTA rate constant.[82] Subsequent theoretical and experimental studies expanded on these findings, clarifying the underlying spin dynamics and validating the role of MFEs in triplet-based luminescence systems.[83, 84] Building on this foundation, Faulkner and co-workers applied magnetic field studies to ECL systems in solution, verifying the presence of a TTA-based emission mechanism in energy-deficient systems. They observed a clear magnetic field dependence in ECL intensity when pairing anion radicals of aromatic hydrocarbons such as anthracene, DPA, rubrene, tetraphenylpyrene (TPP) (Fig. 5A), and fluoranthene with specific cation radicals in N,N-dimethylformamide (DMF). In contrast, no magnetic field effect was seen for energy-sufficient and some marginal systems, such as DPA, TPP anion-cation annihilations, where excited singlet states are directly formed via electron transfer, supporting an S-route mechanism.[85-88] Periasamy et al. later extended this approach to energy-sufficient emitters like rubrene, tetracene, and phenanthrene. They found that the presence of a magnetic field led to sharper ECL pulse decay compared to zero-field conditions, suggesting the participation of triplet intermediates even in thermodynamically sufficient systems.[89]

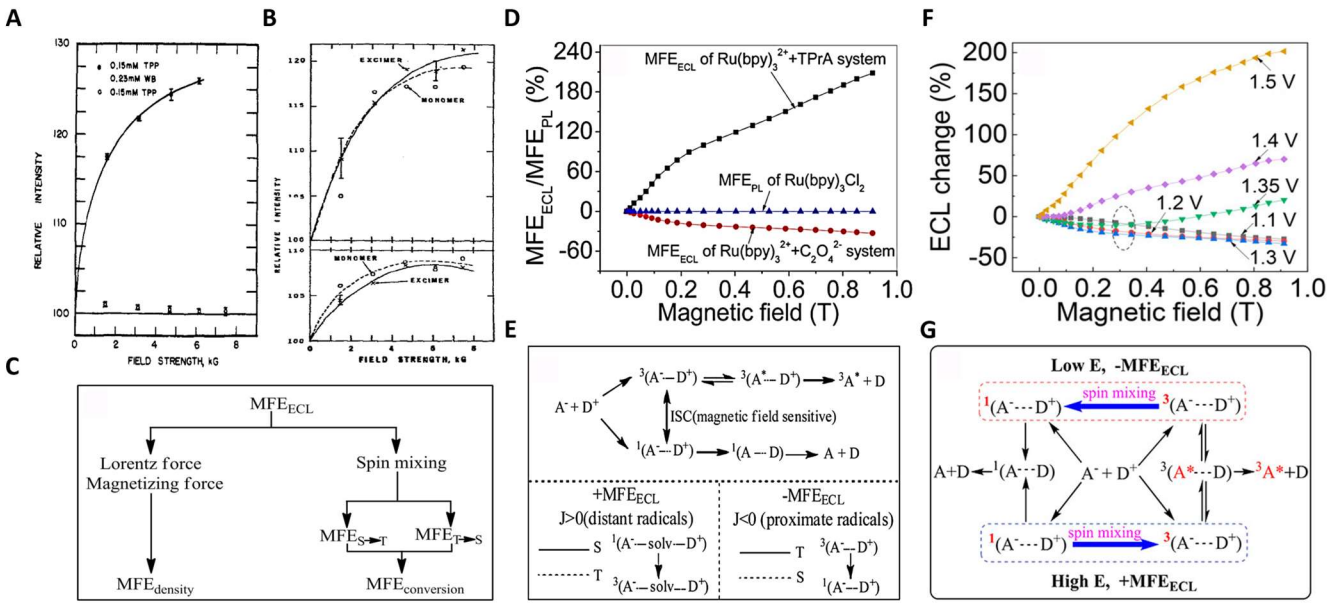



**Fig. 5** Magnetic field effects on (A) luminescence from systems: TPP anion and Wurster's Blue; TPP anion and cation radicals. (B) monomer and excimer ECL in pyrene-based systems. (C) Schematic $MFE_{ECL}$ generation channels. (D) $MFE_{ECL}$ on $Ru(bpy)_3^{2+}$-ECL with two different co-reactants. (E) Magnetic field sensitive reaction mechanism of ECL process. (F) $MFE_{ECL}$ under different applied potentials. (G) Potential-induced inversion of $MFE_{ECL}$ from negative to positive values. (A) Reprinted with permission from ref. 88. Copyright 1972 American Chemical Society. (B)

Reproduced with permission from ref. 91. Copyright 1974 Elsevier B.V. (C) Reprinted with permission from ref. 92. Copyright 2015 Springer Nature. (D)-(E) Reprinted with permission from ref. 93. Copyright 2015 American Chemical Society. (F)-(G) Reprinted with permission from ref. 94. Copyright 2023 American Chemical Society.

In another application, Tachikawa et al. used the magnetic field effect to probe triplet quenching dynamics. In anthracene ECL, a positive magnetic field effect (increased delayed fluorescence with increasing field) was observed when quenching by paramagnetic ions occurred. In contrast, negative MFEs were observed in their absence, indicating that magnetic modulation of triplet–radical ion interactions could provide insight into quenching pathways.[90] Furthermore, Tachikawa used the magnetic field response to distinguish the origin of ECL emissions at different wavelengths. Long-wavelength emissions showed the same field dependence as monomer emissions, see Fig. 5B, supporting their assignment to excimer or exciplex formed via TTA.[91]

In recent work, the $MFE_{ECL}$ parameter was introduced to quantify magnetic field effects on ECL, defined as MFE = $(S_B - S_0)/S_0 \times 100\%$, where $S_B$ and $S_0$ are ECL intensities with and without a magnetic field. Positive and negative values indicate enhancement or suppression of ECL, respectively. Beyond influencing the density of light-emitting states via Lorentz and magnetizing forces on reactant radicals, MFEs have also been observed in spin mixing and spin conversion within intermediate charge-transfer (CT) complexes $[A^{-}\cdots D^{+}]$, as illustrated in Fig. 5C.[92]

Pan et al. explored MFEs in $Ru(bpy)_3^{2+}$ (A) ECL systems and observed opposite magnetic responses depending on the choice of anodic co-reactants (D), see Fig. 5D.[93] They attributed this behaviour to magnetic field-induced spin interconversion between singlet $^1(A^{\cdot}\cdots D^{+})$ and triplet $^3(A^{\cdot}\cdots D^{+})$ radical pairs via intersystem crossing, occurring before the excited states of A* is formed. The differing local magnetic fields experienced by each radical in the pair lead to spin precession, altering their spin alignment between parallel and antiparallel states. Zeeman splitting under the magnetic field reduces the singlet–triplet energy gap (2*J*), enhancing spin conversion. Therefore, the sign of the inter-radical exchange interaction (*J*), which is positive for $[Ru(bpy)_3^{3+}\cdots TPrA^{\cdot}]$ and negative for $[Ru(bpy)_3^{3+}\cdots CO_2^{-\bullet}]$, ultimately determines whether the $MFE_{ECL}$ is positive or negative, as illustrated in Fig. 5E. Additionally, they reported abnormal MFE behaviour during magnetic relaxation, proposing an inverse triplet-to-singlet conversion due to relaxed spin alignment in the charge-transfer complexes.[92] Most recently, a potential-induced transition between negative and positive MFEs was reported in the $Ru(bpy)_3^{2+}$ + oxalate ($C_2O_4^{2-}$) ECL system (Fig. 5F and 5G).[94] This behaviour was attributed to a shift in the dominant radical pairs formed under different applied potentials. At lower potentials, triplet-state $[Ru(bpy)_3^{3+}\cdots CO_2^{-\bullet}]$ pairs prevail, resulting in negative MFEs, whereas higher potentials favor singlet-state $[Ru(bpy)_3^{3+}\cdots Ru(bpy)_3^{+}]$ pairs, leading to positive MFEs. These findings establish a clear link between the electrochemical driving force and spin-state dynamics, offering new insights into the mechanistic control of MFEs in ECL systems.

In summary, the aforementioned theories and methods have been proposed and employed to investigate the ECL mechanisms, and more specifically, to distinguish S-, T- or mixed route for various ECL systems. These methods rely on differences in energetic thresholds, kinetic behaviours, or magnetic field sensitivities associated with triplet states. However, conflicting conclusions often arise when different techniques, such as decay-curve analysis versus magnetic field effect studies, are applied to the same system. These discrepancies are largely attributable to variations in experimental conditions, system composition, or the specific time segment of the light emission pulse being analysed. Unfortunately, research on triplet-involved ECL mechanisms has extensively reduced compared to two decades ago. In recent studies, the interpretation of ECL mechanisms has increasingly relied on the photoluminescence properties of luminophores. Transient PL has been widely used to investigate the involvement of long-lived triplet states by analysing delayed emission components and estimating their lifetimes. While this

technique provides useful insights into triplet dynamics especially in TADF-ECL systems,[41, 95, 96] it remains an indirect and somewhat oversimplified proxy for actual ECL processes, given the fundamental differences between photoexcitation and electrochemical excitation pathways.

# 4. Engineering Triplet-Enabled ECL: Structure–Function Insights

Triplet-involved ECL emitters, including phosphorescent, TADF, and TTA luminophores, have gained significant attention due to their ability to utilise triplet excitons for light emission—substantially enhancing ECL efficiency. These emitters typically feature specific structural motifs designed to promote ISC, RISC, or efficient triplet–triplet interactions. For example, phosphorescent complexes often incorporate heavy metals (e.g., Ru, Ir, Pt, Au) to enhance SOC, while TADF materials adopt a donor–acceptor architecture to spatially separate HOMO and LUMO, thereby reducing the $\Delta E_{ST}$ and facilitating RISC. TTA emitters, on the other hand, require a high triplet yield and appropriate energy alignment for efficient triplet fusion. Additionally, molecular rigidity suppresses non-radiative decay, while aggregation or solid-state packing can either enhance or quench emission depending on the degree of exciton diffusion and intermolecular interactions. Understanding and optimising the structure–function relationships of triplet-involved ECL emitters are essential for advancing their performance in applications such as sensing, imaging, and optoelectronic devices. In this section, we focus on representative materials and molecular architectures that operate via triplet-based mechanisms, specifically highlighting systems exhibiting TTA and TADF mechanisms.

### 4.1 TTA-ECL emitters

TTA emitters have emerged as promising luminophores in ECL due to their ability to harvest triplet excitons without requiring heavy atoms, enabling efficient light emission through purely organic systems. This mechanism allows for high photoluminescence quantum yields and reduced energy losses, making TTA-based systems attractive for low-voltage, high-efficiency ECL applications.To achieve effective TTA in ECL, luminophores must meet key structural criteria: (1) a sufficiently long-lived triplet state to enable diffusion and annihilation; (2) the energy of two triplets higher than that of the singlet ($2T_1 > S_1$) to enable efficient upconversion; and (3) high triplet yield upon electrochemical excitation. To meet the requirements, TTA emitters typically possess a large, conjugated structure, such as polyaromatic hydrocarbons, which exhibits π-electron delocalization across the molecular framework facilitating the stabilization and diffusion of triplet excitons, allowing efficient energy migration and transfer, and high rigidity that reduces vibrational energy loss (nonradiative decay). Typical TTA-ECL emitters and corresponding electrochemical properties and energy levels were summarised in Fig. 6 and Table 1, respectively. Additionally, molecular packing and solid-state organization often play critical roles in promoting exciton diffusion and minimizing non-radiative decay.

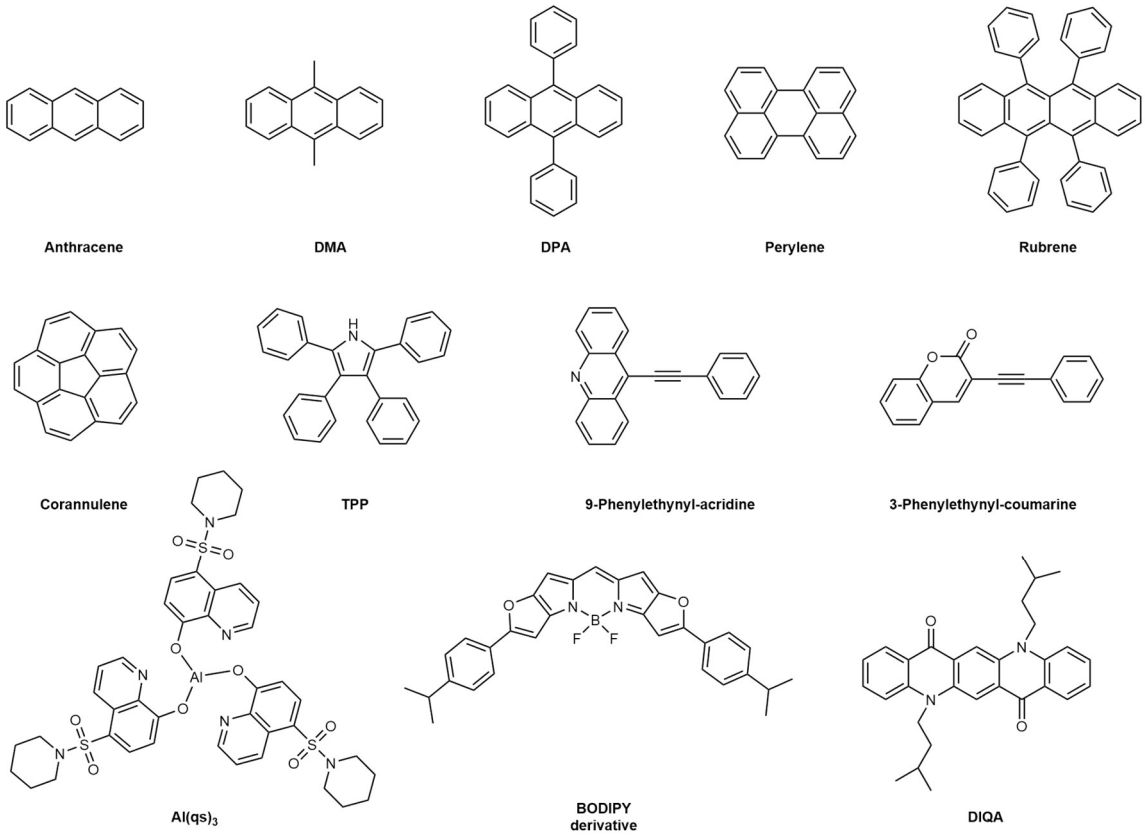



**Fig. 6** Molecular structures of published TTA-ECL emitters.

**Table 1** ECL maxima, redox potentials, reaction enthalpies of radical ion annihilation, singlet and triplet energies and related energy gap ($\Delta E = 2E_{T_1} - E_{S_1}$) for typical TTA-ECL emitters previously reported.

| ECL emitters | $\lambda_{max}$ECL nm (eV) | $E_{p,OX}$ /V[a] | $E_{p,RED}$ /V[a] | $-\Delta H^o$/eV | $E_{S_1}$/eV | $E_{T_1}$/eV | $\Delta E$/eV |
|---|---|---|---|---|---|---|---|
| Rubrene[26, 88, 97] | 570 (2.18) | 0.82 | -1.41 | 2.07[b] | 2.23 | 1.14 | 0.05 |
| Anthracene[25, 26, 88, 98] | 400, 425 (3.10, 2.92) | 1.20 | -1.94 | 3.04[b] | 3.30 | 1.78 | 0.26 |
| DMA[99] | 430 (2.88) | 0.81 | -2.60 | 3.31 | 3.15 | 1.75 | 0.35 |
| DPA[26, 88, 97] | 430 (2.88) | 1.19 | -1.84 | 2.87[b] | 3.08 | 1.65 | 0.22 |
| Perylene[100] | 475 (2.61) | 1.03 | -1.72 | 2.55 | 2.85 | 1.56 | 0.27 |
| Corannulene[101] | - | 0.15 (TMDPA)[c] | -1.90 | 1.95 | 2.93[d] | - | - |
| TPP[29, 88] | 397 (3.12) | 0.90 | -2.78 | 3.52 | 3.49 | 2.48 | 1.47 |
| 9-Phenylethynylacridines[33] | 473~534 (2.32~2.62) | 0.98~1.67 | -0.81~-0.87 | 1.67~2.38 | 2.18~2.88[d] | - | - |
| 3-Phenylethynylcoumarins[34] | 438~505 (2.45~2.83) | 0.90~1.95 | -0.88~-0.93 | 1.62~2.72 | 2.25~3.05[d] | - | - |
| QIDA[32] | 532 (2.33) | - | - | 2.28[b] | 2.32 | 1.78 | 1.24 |
| $Al(qs)_3$[32] | 515 (2.41) | - | - | 2.13 (TPD)[c] | 2.47 | 2.12 | 1.77 |
| BODIPY derivative[35] | 670 (1.85) | 0.88 | -0.78 | 1.50[b] | 2.00[e] (1.85[d]) | 0.99[e] | -0.02 |

[a] Potential values as reported or converted *vs* SCE;
[b] Estimated according to $-\Delta H^o = E_{p,OX} - E_{p,RED} - 0.16$ eV;[34]
[c] Reported $-\Delta H^o$ or $\Delta E_1/_2$ values vary depending on the coreactant; data shown corresponds specifically to the coreactant indicated in brackets;
[d] Calculated from reported spectral data according to $E_{S_1} = 1240 \times 2/(\lambda_{abs} + \lambda_{flu})$;
[e] Obtained by TD-DFT simulation.

Rubrene is a typical TTA emitter that has been detailed in earliest ECL studies owing to stable radical ions, rapid annihilation and energy deficiency to directly generate triplets in aprotic media.[97] Additionally, solid-state rubrene microstructures also exhibit TTA ECL emission and it strongly relies on the polymorphism. Gu et al. showed that reprecipitation conditions control molecular stacking arrangements in these polymorphs: low supersaturation yields tightly packed triclinic 1D microwires, while high supersaturation produces loosely packed monoclinic 2D hexagonal plates (Fig. 7A and 7B).[102] These polymorphs exhibit different π–π interactions, affecting charge transport, nonradiative decay, and exciton dynamics. The triclinic phase offers better charge mobility but higher nonradiative quenching, reducing TTA efficiency. In contrast, the monoclinic phase, with weaker interactions, supports longer triplet lifetimes and higher fluorescence yields, favouring more efficient TTA-ECL, as shown in Fig. 7C and 7D.

Anthracene-type emitters, such as anthracene, DMA, and DPA share a tricyclic core, exhibiting similar photophysical properties: high fluorescence quantum yields, micro- to millisecond triplet lifetimes in deaerated media, and positive $\Delta E$ values ($\Delta E = 2E_{T_1} - E_{S_1}$), favouring TTA. Their respective energy levels were listed in Table 1. In anthracene, the energy from radical ion recombination (~3.1 eV) is slightly below $S_1$, making direct singlet formation endothermic and favouring TTA.[25, 26] DMA's methyl groups lower $S_1$ and slightly stabilise the radical cation, modestly enhancing $\Delta E$ but still favouring monomer emission unless under strong fields or heat.[99] DPA's phenyl groups extend conjugation and introduce steric hindrance, reducing excimer loss and steering encounters toward productive annihilation.[97] Its stabilised radical ions sustain a large triplet population even at low voltages.

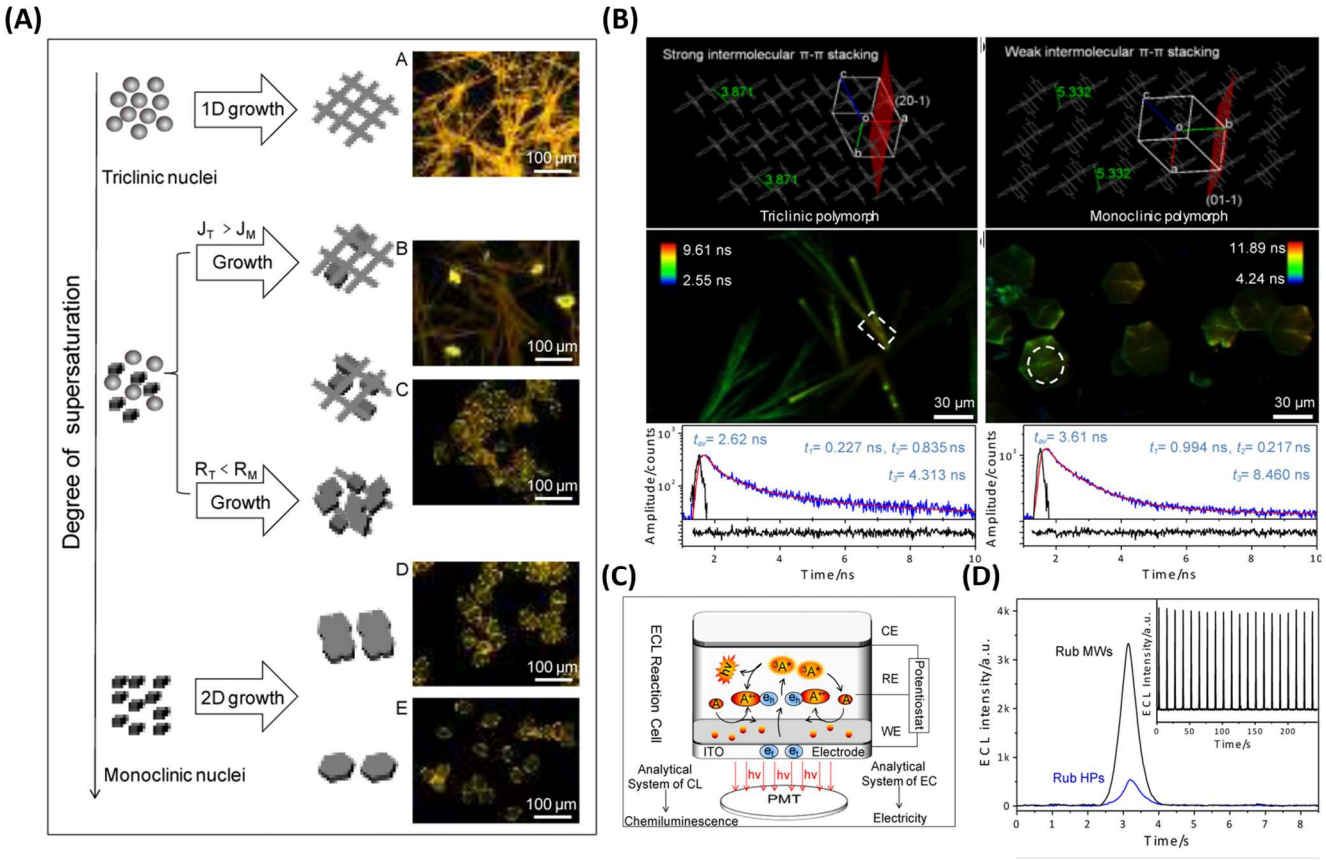



**Fig. 7** (A) Schematic depiction of formation mechanism and (B) molecular stacking, and fluorescence decay curves of two rubrene crystal structures: triclinic and monoclinic crystals. (C) The reaction cell for ECL measurement. (D) ECL performance comparison of the two stacking structures. Reproduced with permission from ref. 102. Copyright 2017 American Chemical Society.

Perylene, with its extended five-ring π-conjugated structure, effectively lowers the singlet ($S_1 \approx$ 2.85 eV) and triplet ($T_1 \approx$ 1.56 eV) energy levels while maintaining the energetic requirement for TTA ($2T_1 > S_1$). This molecular configuration favours triplet generation through annihilation, as the energy released by radical ion recombination (2.3–2.6 eV) is insufficient for direct singlet formation but sufficient to populate the triplet state.[100] The structural rigidity and planarity of perylene minimize excimer formation, enabling clean, well-defined fluorescence spectra, which is particularly advantageous for ratiometric sensing. Residual long-wavelength emission is now attributed to degradation products of the relatively unstable perylene cation, underscoring the importance of radical ion stability for maintaining spectral purity.

Across anthracene-based systems, subtle variations in conjugation, steric effects, and energy levels result in diverse TTA-ECL behaviours. Anthracene engages the TTA route only under high fields, DMA requires thermal or electric activation, DPA achieves near-quantitative singlet formation, and perylene operates predominantly via TTA under energy deficient conditions.[77] These differences reflect how intertwined energetic alignment, molecular packing, and radical stability shape the efficiency of triplet-fusion-based ECL, offering valuable guidance for designing advanced luminophores.

Furthermore, Marcaccio et al. demonstrated the first-time use of corannulene, a rigid, bowl-shaped $C_{60}$ fragment with 20 conjugated π-bonds in blue-light ECL emission. It possesses a low-lying LUMO (first reversible reduction at –1.9 V *vs* SCE) and a comparatively deep HOMO, rendering direct oxidation highly positive (~+1.9 V) and kinetically hindered. Due to the instability of its radical cation, excited states are instead accessed via coreactant pathways.[101] Coreactants such as benzoyl peroxide, triarylamines, and *N,N,N′,N′*-tetramethyl-*p*-phenylenediamine (TMPDA) have been employed to generate oxidative radicals that undergo annihilation with corannulene radical anions, producing ECL. Notably, for TMPDA, the redox gap is insufficient to directly populate the singlet excited state (CA*). Instead, electron exchange leads to population of the lowest triplet state, with light emission proceeding via TTA. The rigid, geodesic structure of corannulene localises spin density at the rim, stabilising both the radical anion and the triplet state. This architecture prolongs triplet lifetimes and positions $2T_1$ only slightly above $S_1$, rendering annihilation exergonic and enabling efficient TTA-ECL under energetically deficient conditions.

In addition to polyaromatic hydrocarbons, various aromatic heterocycles—such as tetraphenylpyrrole (TPP) and tetraphenylthiophene (TPT)—have also been reported to exhibit ECL via the TTA mechanism, particularly in mixed systems.[29] Donor-substituted phenylethynylacridines, as systematically modified by Ho et al, was demonstrated exhibiting ECL via a TTA mechanism under energy deficient conditions, with annihilation enthalpies (1.7–2.4 eV) lower than the optical singlet energies (2.3–2.6 eV) but remain higher than the triplet levels.[33] The acridine core stabilises the LUMO relative to anthracene due to the electron-withdrawing ring nitrogen. Tuning the donor strength at the phenylethynyl position modulates the electronic structure without disrupting the TTA process: weaker donors retain frontier orbital localisation on the acridine core and promote excimer-like aggregation, preserving triplet accessibility; stronger donors, like N,N-dimethylamino groups, raise the HOMO onto the peripheral phenyl ring, introducing charge-transfer character and narrowing the energy gap. Additionally, the sp-hybridised ethynyl linker extends conjugation, reduces the reduction potential (~0.8 V), and imparts structural rigidity, which suppresses internal conversion and prolongs triplet lifetimes. The resulting π-extended framework supports π–π stacking, as evidenced by the 3.59 Å interplanar distance between offset acridine units in the crystal structure of the dimethylamino derivative. This slip-stacked geometry facilitates triplet diffusion, enhances exciton fusion, and promotes molecular aggregation, contributing to solid-state fluorescence and blue-shifted ECL. Similarly, for the 3-substituted phenylethynylcoumarins where the almost planar conformation resulting in a delocalised HOMO and LUMO that span the extended π-system

and reduces the annihilation enthalpy (1.6–2.7 eV), the close packing particularly in concentrated ECL solutions, due to the head-to-head π-stacked arrangements with interplanar spacing of approximately 3.6 Å, facilitates rapid triplet hopping between molecules until annihilation occurs within transient H-type or trans-excimer-like cages, where non-radiative losses are minimised and TTA efficiency is maximised.[34] In contrast, 7-substituted analogues adopt a nearly orthogonal geometry, disrupting conjugation and localising the HOMO and LUMO on separate moieties. The reduced orbital overlap and less favourable packing lower TTA efficiency, even though the polarised C ≡ C linker still stabilises radical ions. Additionally, electron-donating groups like N,N-dimethylaniline or methoxy lower the donor's oxidation potential and extend radical cation lifetimes, enhancing diffusion and recombination with complementary radicals to support TTA emission without external co-reactants.

Beyond these, several OLED emitters have been successfully repurposed for TTA-based ECL, especially under energy-deficient conditions where direct $S_1$ formation is energetically inaccessible. Notable examples include a sulfonamide derivative of tris(8-hydroxyquinoline) aluminum ($Al(qs)_3$) and a bis(isoamyl) quinacridone derivative (DIQA), both of which display delayed fluorescence and follow second-order annihilation kinetics—hallmarks of TTA.[32] Ishimatsu et al. later introduced a BODIPY derivative featuring extended π-conjugation and a fused heteroaryl framework.[35] This molecular architecture was designed to modulate both electronic and excitonic properties, reduce spin density on radical ions to enhance cation stability, and introduce steric hindrance to suppress non-radiative losses such as excimer formation, and also support efficient Dexter-type energy transfer that is essential for TTA. As a result, the BODIPY derivative maintained high fluorescence quantum yield ($\Phi_{FL}$) while enabling effective triplet formation and controlled annihilation dynamics in ECL.

### 4.2 TADF-ECL emitters

Achieving 100% quantum efficiency in TADF-ECL systems hinges on efficient triplet-to-singlet conversion via RISC under electrochemical conditions. Most TADF emitters adopt a donor–acceptor (D–A) architecture, where spatially separated HOMO on the donor and LUMO on the acceptor, form a charge-transfer (CT) state reducing $\Delta E_{ST}$ and facilitating RISC. In the ECL environment, molecular stability is equally critical; tailored substituents to the core structure can modulate charge distribution, stabilise radical ions, mitigate parasitic reactions and ensures robust redox reversibility essential for sustained emission. The structure and ECL-related properties of typical TADF-ECL emitters are summarised in Fig. 8 and Table 2, respectively.

**4.2.1 D-A architecture and molecular tuning.** In 2014, Ishimatsu and coworkers reported a pioneering breakthrough in ECL, demonstrating that donor–acceptor TADF emitters mainly consisted of a mono- or dicyanobenzene acceptor core and varied number of carbazole donor groups, such as 2CzPN, 4CzPN, 4CzIPN, and 4CzTPN, achieved ECL efficiencies comparable to their photoluminescence quantum yields (PLQYs).[36] Among them, 4CzIPN possessing 1,3-dicyanobenzene acceptor and four carbazole donors, reached an impressive 47% $\Phi_{ECL}$ in dichloromethane, which closely matches its 54% PLQY and far surpassing the ~5–6% typical of $Ru(bpy)_3^{2+}$. This work underscores TADF's promise for high-efficiency, metal-free ECL systems.

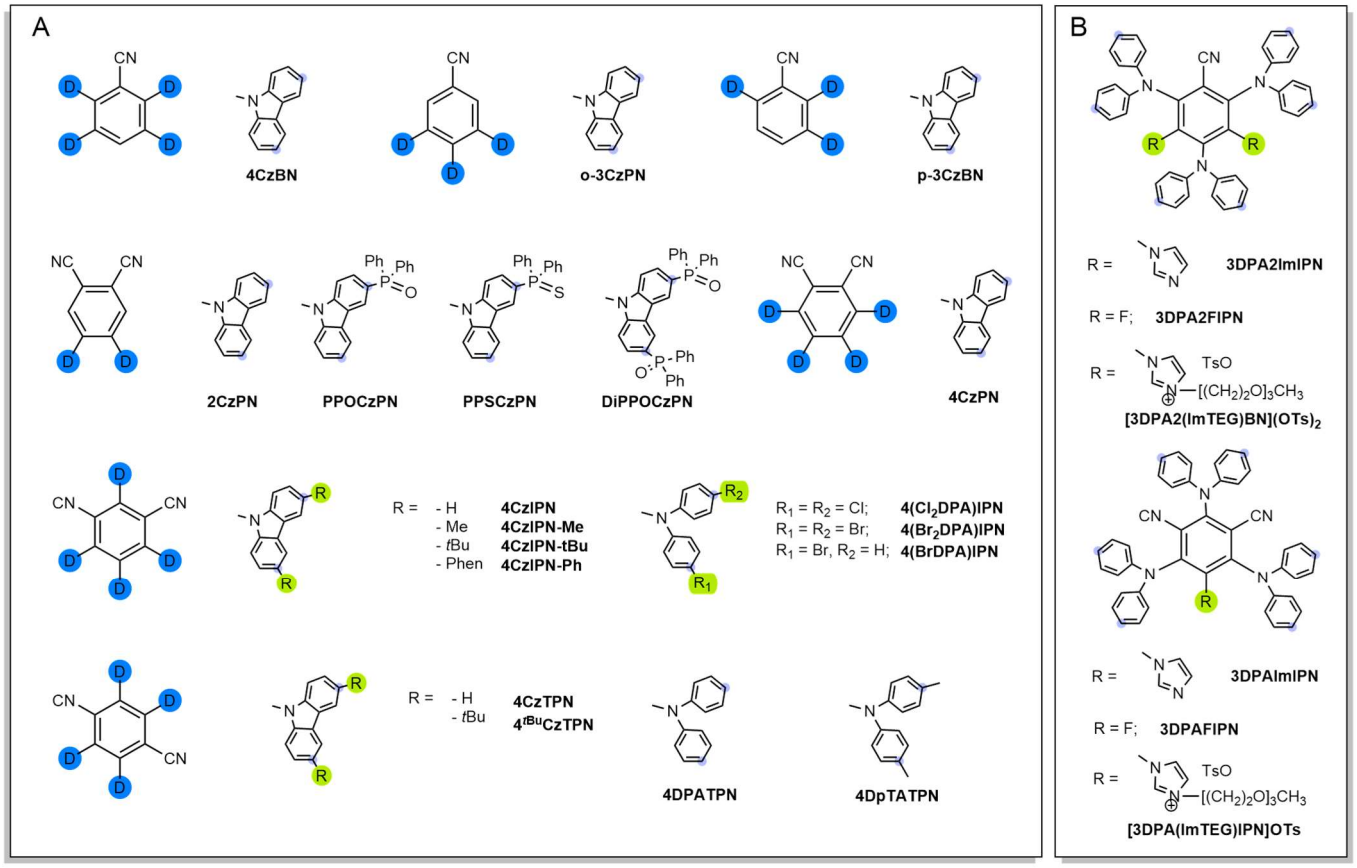



**Fig. 8** Molecular structure of mono- and dicyanobenzene based TADF ECL molecules with modification of (a) the electron-donating groups, (b) cyanoarene accepting core.

Building on this design, recent efforts have been focused on dicyanobenzene-based TADF architectures. Compared to mono-cyano acceptors,[103] incorporating an additional cyano group strengthens the electron-accepting ability, lower the LUMO energy and further reduces $\Delta E_{ST}$. The placement of the two cyano groups, typically at the 1,3- or 1,4-positions, ensures that the HOMO remains localized on the donor units. As highlighted in a review by Cao et al.,[104] strategies such as adding multiple cyano groups or introducing cyano-substituted heteroaromatic acceptors effectively enhance acceptor strength in TADF systems. Consequently, multi(carbazolyl)-dicyanobenzene structures have become a dominant motif in ECL emitter design due to their favourable photophysical properties.

In 2016, Imato and co-workers investigated how donor substituents affect ECL performance and operational stability of the TADF emitters.[105] They synthesized 4CzIPN derivatives bearing methyl (4CzIPN-Me), tert-butyl (4CzIPN-tBu), and phenyl (4CzIPN-Ph) groups on the carbazolyl donors. All exhibited yellow to orange delayed fluorescence, with 4CzIPN-tBu achieving ~40% $\Phi_{ECL}$ in DCM, comparable to unsubstituted 4CzIPN. Bulky tert-butyl and phenyl groups also helped stabilise ECL by sterically blocking reactive sites and delocalising the spin density, effectively suppressing radical-induced polymerisation. However, the improved stability was accompanied by a moderate decline in ECL efficiency, underscoring the inherent trade-off between durability and performance in TADF-based ECL systems. Zysman-Colman's group in 2022 developed derivatives of 2CzPN (PPOCzPN, PPSCzPN, and DiPPOCzPN) featuring phenoxathiin (PPO) or phenothiazine (PPT) donors.[95] These emitters maintained high ECL efficiencies while shifting emission maxima into the deep blue ($\lambda_{ECL}$ ~420–440 nm), a long-standing challenge in TADF-ECL due to the need for large energy gaps and small $\Delta E_{ST}$. This design highlights how strategic donor

modification, which preserves the D–A core while adjusts conjugation and electron-donating strength, can tailor emission colour without compromising triplet harvesting.

**Table 2.** ECL maxima, electrochemical, photophysical properties and singlet-triplet energy gap of cyanobenzene based TADF ECL emitters.

| ECL emitters | $\lambda_{ECL}$max nm | $E_{p,\,ox}$ V | $E_{p,\,RED}$ V | $\Phi_{ECL}$ % | $k_p^{-1}$ ns | $k_d^{-1}$ $\mu$s | $\Phi_{PL}$ % | $\Delta E_{ST}$ eV | Ref |
|---|---|---|---|---|---|---|---|---|---|
| 4CzIPN-Me | 585 | - | -1.23 | 13 | 20 | 2.1 | 38 | 0.307 | Ref. 105 |
| 4CzIPN-tBu | 572 | 1.42 | -1.21 | 35 | 20 | 2.4 | 44 | 0.308 | |
| 4CzIPN-Ph | 595 | 1.41 | -1.15 | 13 | 13 | 1.5 | 17 | 0.214 | |
| 4CzIPN | 555 | 1.52 | -1.21 | 47 | 24.6 | 2.04 | 54 | 0.345[105] | Ref. 106 |
| 4CzPN | 595 | - | -1.16 | 14 | 17.8 | 5.03 | 29 | - | |
| 4CzTPN | 600 | - | -1.02 | 6 | 6.5 | 1.46 | 15 | - | |
| 2CzPN | 550 | 1.47 | -1.45 | 4.5 | 33.3 | 20 | 34 | 0.32[95] | |
| PPOCzPN | 520 | 1.59 | -1.24 | 17* | 6.1 (43), 20.0 (57) | 9 (3), 146 (22), 1024 (75) | 51 | 0.21 | Ref. 95 |
| PPSCzPN | 500 | 1.76 | -1.32 | 6* | 5.8 (44), 13.6 (56) | 5 (0.5), 174 (10), 1361 (90) | 47 | 0.22 | |
| DiPPOCzPN | 475 | 2.06 | -1.24 | 1* | 6.7 (40), 14.1 (60) | 5 (2), 69 (6), 1176 (92) | 61 | 0.27 | |
| 4CzBN | 539 | - | - | 1.63 | 287.47 | 4.03 | 42.42 | 0.09 | Ref. 103 |
| o-3CzBN | 464 | - | - | 1.44 | 18.78 | 0.05 | 26.52 | 0.16 | |
| p-3CzBN | 457 | - | - | 0.84 | 6.15 | 0.25 | 22.6 | 0.1 | |
| 4DPATPN | 597 | 1.03; 1.26 | -1.39 | 1.72 | 2.08 | 16.53 | 49.2 | - | Ref. 107 |
| 4DpTATPN | 625 | 0.86; 1.04 | -1.46 | 0.33 | 2.32 | 7.19 | 15.0 | - | |
| 4tBuCzTPN | 593 | 1.44 | -1.09 | 0.3 | 3.66 | 1.91 | 6.6 | - | |
| 4(BrDPA)IPN | 532 | 1.14 | -1.52 | 0.11 | 1.4 | 20 | 15 | 0.273 | Ref. 108 |
| 4($Cl_2$DPA)IPN | 530 | 1.21 | -1.45 | 0.98 | 2.3 | 47 | 37 | 0.269 | |
| 4($Br_2$DPA)IPN | 528 | 1.24 | -1.41 | 1.27 | 1.3 | 12 | 21 | 0.255 | |
| 3DPAFIPN | 526 | 1.24 | -1.59 | 0.43 | - | - | - | 0.39 | |
| 3DPA2FBN | 482 | 1.25 | -1.85 | 0.16 | - | - | - | 0.361 | |
| 3DPAImIPN | 534 | 1.35 | -1.49 | 0.82 | 5.18 | 49.6 | 32.5 | 0.337 | |
| 3DPA2ImBN | 514 | 1.35 | -1.68 | 1 | 7.01 | 26.4 | 35.7 | 0.303 | |
| C[3]A@o-DCB | - | - | - | - | 133.39 | 2.21 | 39.21 | 0.01 | Ref. 109 |
| C[3]A@p-DCB | - | - | - | - | 137.06 | 5.81 | 50.40 | 0.011 | |
| C[3]A@m-DCB | - | - | - | - | 363.87 | 8.86 | 72.46 | 0.006 | |

* Relative efficiency *vs* standard $Ru(bpy)_3^{2+}$ annihilation ECL.

More recently, Fracassa et al. reported a series of diphenylamine–dicyanobenzene emitters featuring halogenated donors.[106] Halogen substituents (F, Br, I) subtly reduce donor strength and enhance spin–orbit coupling, tuning the singlet–triplet gap and RISC kinetics. This led to progressively higher ECL efficiencies in the order H < Br < I. On the acceptor side, dicyanobenzene cores were functionalised with fluorine or N-heterocycles (e.g., imidazole) to adjust emission color and solubility. Notably, imidazole-functionalisation enabled the attachment of hydrophilic triethylene glycol chains, producing water-dispersible TADF emitters without compromising their core photophysics.

**4.2.2 Supramolecular with through-space charge transfer (TSCT).** Beyond conventional molecular tuning, supramolecular design has emerged as an effective tool to enforce the twisted D–A geometry critical for TADF. One way involves extending the traditional D–A framework to include through-space charge transfer (TSCT) architectures, where charge transfer occurs via π–π interactions rather than direct covalent linkage. By strategically engineering these through-space D–A interactions and finely controlling the spatial molecular arrangement, researchers can substantially enhance triplet harvesting and suppress non-radiative losses, ultimately leading to improved ECL intensity and operational stability.

A key example is TPA-ace-TRZ, developed by Zysman-Colman's group in 2021 and adapted for ECL in 2023.[107, 108] This emitter features a triphenylamine (TPA) donor and triazine (TRZ) acceptor aligned in a pseudo-cofacial geometry via a rigid acenaphthylene bridge. The highly twisted D–A arrangement minimises frontier orbital overlap, resulting in a small $\Delta E_{ST}$ (< 100 meV) that facilitates efficient RISC. The rigid spacer also suppresses non-radiative decay and stabilises charge-separated states, leading to a PLQY of ~75% and $\Phi_{ECL}$ of ~43% in acetonitrile. Further functionalisation of the acenaphthylene core has yielded TSCT-TADF emitters theoretically capable of harvesting nearly 100% of triplet excitons.

Building on this concept, host–guest TADF co-crystals offer another elegant supramolecular TSCT strategy. Zheng et al. recently demonstrated that incorporating aromatic acceptor guests (e.g., dicyanobenzene derivatives) into a rigid donor host lattice forms crystalline materials with locked D–A geometries.[109] These co-crystals exhibited significantly enhanced ECL intensity and bright green-blue TADF emission compared to their monomeric components. The improved performance was attributed to restricted non-radiative decay and stabilised charge-transfer excitons, highlighting the synergistic effects of spatially constrained donor–acceptor interactions. MOFs have also been integrated to achieve precise spatial organization of D and A units. A 2024 study reported the incorporation of phenyl-carbazole derivatives as donor guests within an acceptor-based MOF, enabling aligned TSCT pathways.[110] This spatially controlled assembly led to a marked increase in ECL efficiency, emphasising how structural enforcement of twisted D–A geometry can maximise triplet upconversion and light emission.

**4.2.3 D-A TADF polymers.** Donor–acceptor TADF polymers represent a rapidly advancing class of ECL emitters, offering solid-state processability, robust electrochemical behaviour and efficient triplet utilization. A notable early example is named PCzAPT10, reported by Niu's group., which contains a 9,9-dimethylacridan donor in the main chain and pendant triazine acceptors in each repeat unit.[40] The acridan-based donor in the backbone provides a high triplet energy and a twisted geometry, while the triazine on the side chain serves as a strong acceptor, together yielding a small $\Delta E_{ST}$. In thin films, PCzAPT10 exhibited clear TADF character (delayed fluorescence) and a high PLQY, indicating efficient RISC in the solid state. Impressively, TADF polymer showed high relative $\Phi_{ECL}$ up to 194% *vs* the $Ru(bpy)_3^{2+}$/TPrA system. Additionally, the incorporation of robust electroactive units in PCzAPT10 mitigates electrode fouling and irreversible oxidation, as evidenced by its reversible redox behaviour in cyclic voltammetry. This stability enables both annihilation and co-reactant ECL modes.

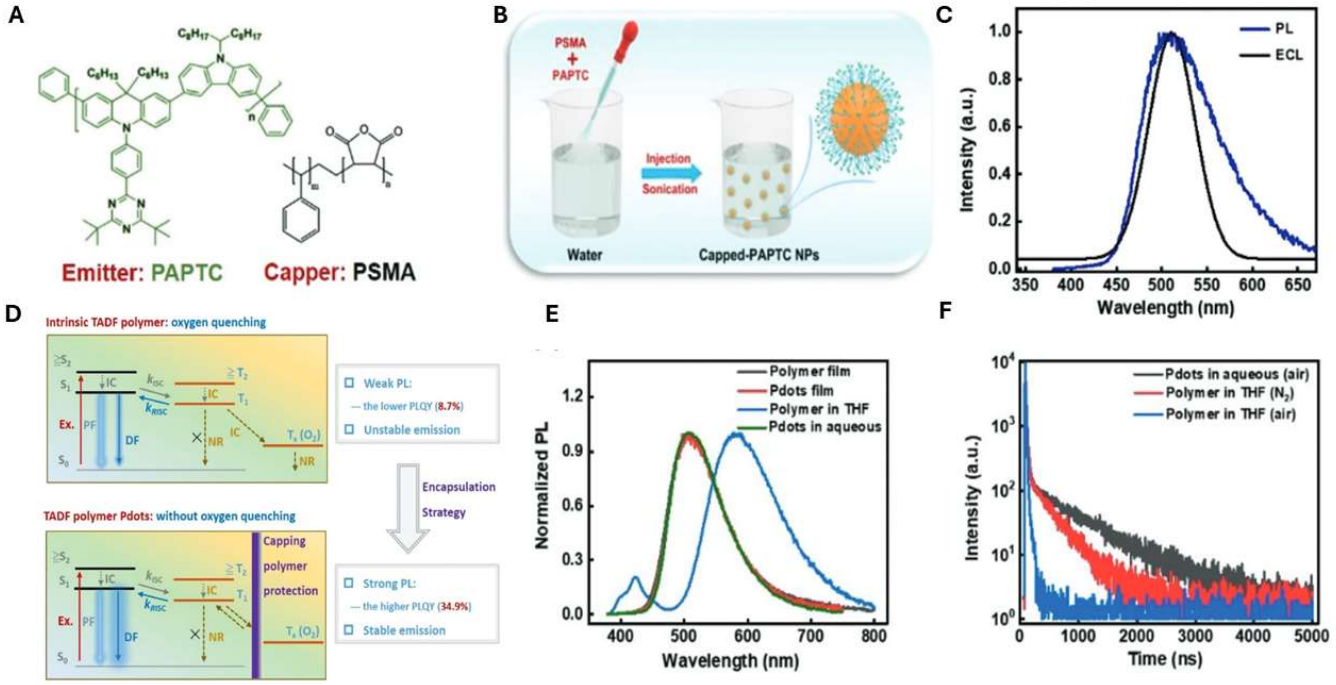



**Fig. 9** (A) A schematic illustration of the capped TADF polymer PAPTC dots (Pdots). (B) Chemical structures of the PAPTC emitter and PSMA capper. (C) PL spectrum (blue line) of Pdots film and ECL spectrum (black line) of Pdots/40 mM $C_2O_4^{2-}$ couple. (D) A comparison of the photophysical process of intrinsic TADF polymer. (E) Steady-state PL and (F) transient PL results of PAPTC polymer under different conditions. Reproduced with permission from ref. 96. Copyright 2022 Royal Society of Chemistry.

Building on this, Niu's group developed PAPTC (Fig. 9A), a conjugated polymer with alternating donor units (carbazole and 9,10-dihydroacridine) on the backbone and triazine acceptor units attached to phenyl side chains.[96] This structural configuration achieves spatial separation of HOMO and LUMO minimising orbital overlap and forms a twisted intramolecular charge transfer (TICT) state. They applied a nanoprecipitation protocol as depicted in Fig. 9B: a THF solution of PAPTC is swiftly injected into an aqueous medium containing poly(styrene-alt-maleic anhydride) (PSMA), and brief sonication promotes nucleation, yielding core–shell polymer dots whose PSMA corona provides colloidal stability while serving as an effective barrier to dissolved oxygen during ECL (Fig. 9C and 9D). Encapsulation into polymer dots (Pdots) mitigated aggregation-induced quenching (AIQ) and oxygen quenching and further reduced $\Delta E_{ST}$ from 0.13 to 0.04 eV boosting RISC ($k_{RISC}$ ~1.5 × $10^6$ $s^{-1}$), thereby preserving the TADF character and enhancing ECL in aqueous media, see Fig. 10E and 10F. Wang et al. demonstrated the first water-phase ECL from water-dispersible TADF polymer dots, marking a step toward biofriendly ECL probes despite modest efficiencies (<1%).[111]

**4.2.4 Multi-resonance (MR) TADF materials.** Multi-resonance TADF (MR-TADF) emitters are an emerging class of luminophores that achieve TADF through localized resonance effects rather than conventional D–A geometries. Typically based on boron/nitrogen-doped polycyclic frameworks, these rigid molecules feature alternating electron-rich and electron-deficient atoms within a π-conjugated backbone. This design enables narrowband emission, high PLQY, and a small singlet–triplet energy gap, all while minimizing structural relaxation.

To improve solid-state performance, Zysman-Colman et al. developed $Mes_3$DiKTa, an MR-TADF emitter derived from DiKTa.[112] Incorporating bulky mesityl groups orthogonal to the core, this structure introduces substantial steric hindrance, effectively suppressing π–π stacking and aggregation. As a result, $Mes_3$DiKTa achieves an 80% PLQY in doped thin films, narrow emission spectra, and a small Stokes shift—ideal properties for ECL applications. Yang et al. reported BN-MOPV, a di-boron emitter featuring two MR cores linked by a planar oligophenylene bridge, see Fig. 10A.[113] The molecule displays reversible redox behaviour via two distinct one-electron processes. However, its annihilation ECL was weak due to insufficient energy from electron–hole recombination to access the high-energy emissive state—a common limitation for rigid MR-TADF systems with elevated $S_1$ levels. This underscores the need to match redox energetics with emission requirements in MR-TADF-based ECL designs. Instead, selected coreactants such as BPO and TPrA significantly enhanced the ECL intensity of BN-MOPV (Fig. 10B–D), with ECL efficiency increasing from 11% (via annihilation) to 51% particularly with TPrA, attributed to the greater stability of the generated radicals.

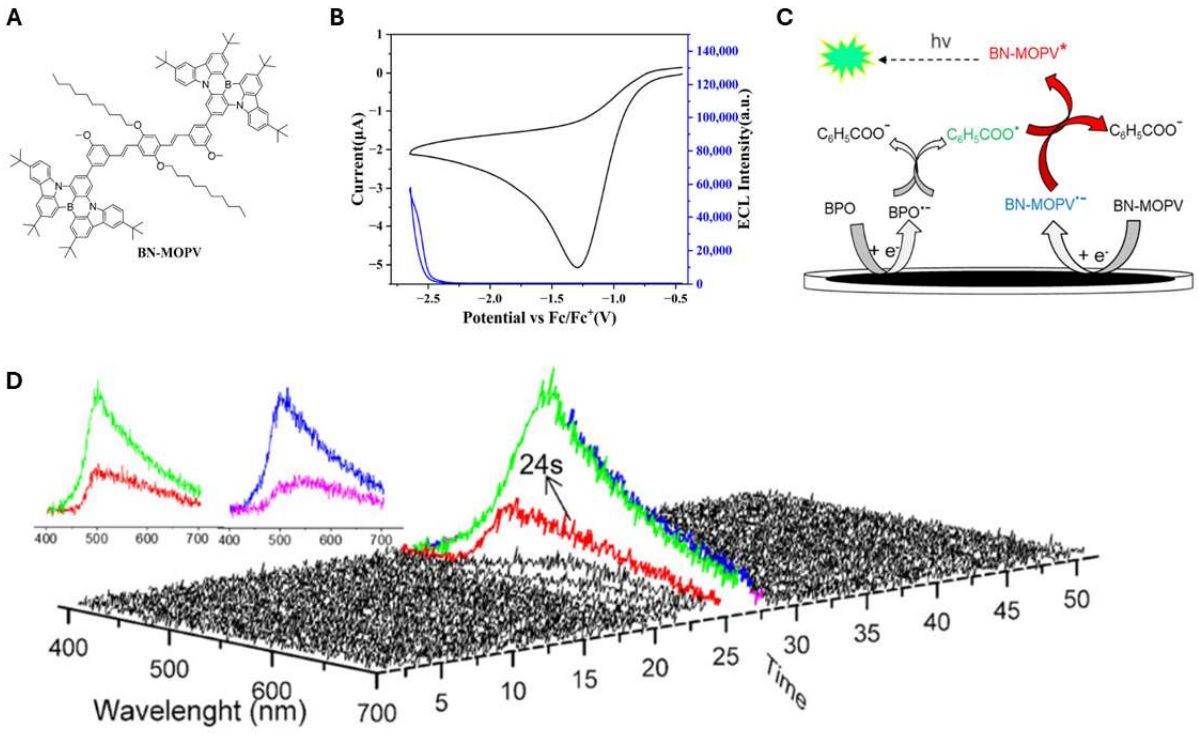



**Fig. 10 (**A) Molecular structure of BN-MOPV. (B) CV and corresponding ECL-voltage curves for BN-MOPV in the presence of BPO. (C) The proposed mechanism of the BN-MOPV /BPO system. (D) Spooling ECL spectra of the BN-MOPV /BPO system Reprinted with permission from ref. 113.

# 5. Applications and Challenges

In recent years, the intensive development of triplet-active ECL emitters and systems, has expanded the use of this technique in high-performance bioanalysis, light-emitting devices and smart electronics.[114-119] While most studies still rely on heavy-metal-based phosphorescent emitters, notable progress has also been made in exploring alternative triplet-involved ECL mechanisms as forementioned. Han et al developed three types of porphyrin dots (TCPP, ZnTCPP, and pMOF) as efficient near-infrared ECL luminophores.[120] By emitting via a TTA mechanism, TCPP dots show up to 56-fold higher efficiency than

$Ru(bpy)_3^{2+}$ standard in the coreactant ECL. A label free "signal-on" ECL biosensor coupling TCPP dots with a $Pb^{2+}$-dependent DNAzyme system and hybridization chain reaction (HCR) amplification was thus developed, achieving ultrasensitive $Pb^{2+}$ detection with a low detection limit of 1.2 $pmol \cdot L^{-1}$. Compared to TTA, TADF emitters have attracted more application trials in ECL sensing, due to theoretically 100% excitons harvesting yield. Polymer dots (Pdots) using a D-A type TADF polymer (poly(TMTPA-DCB)) was developed via nanoprecipitation by Wang et al, see Fig. 11A, achieving theoretically maximum $\Phi_{ECL}$ of 73.7%, 6.27-fold higher than that of conventional fluorescent Pdots (PFBT Pdots).[111] The excellent performance stems not only from the high exciton yield, but also from highly stable negative-charged state in cathodic ECL and oxygen quenching resistance. Combining the TADF Pdots with a rolling circle amplification (RCA) strategy as illustrated in Fig. 11A, a sensitive ECL biosensor was constructed for detecting DNA methylation in the RASSF1A gene, achieving detection limits down to 60 fM and differentiating methylation site locations (Fig. 11B). Similarly, Zou et al. developed TADF polymer dots (PABPC5-Pdots) achieving a 1.39-fold higher ECL efficiency than conventional fluorescent Pdots (F8BT-Pdots), leveraging the advantages of stable anionic radical formation and strong resistance to oxygen quenching.[121] An ECL sensor based on PABPC5-Pdots was constructed for $Cu^{2+}$ detection, achieving a low detection limit of 0.16 nM with excellent stability and selectivity in aqueous environments. Liu et al. developed near-infrared (NIR) ECL nanoparticles based on a TADF emitter with a donor–π–acceptor–π–donor (D-π-A-π-D) structure, named TPA-DCPP, significantly enhancing ECL intensity compared to conventional NIR fluorophores.[122] Leveraging these properties, a sensitive ECL resonance energy transfer (ECL-RET) biosensor was constructed by integrating TPA-DCPP nanoparticles with exonuclease III-assisted polymerase cascade amplification. The resulting biosensor demonstrated ultrahigh sensitivity for circulating tumor DNA (ctDNA) detection, achieving a remarkably low detection limit of 23 nM. Recent studies on AIECL have also demonstrated its effectiveness in biosensing applications. He et al. reported a Pt(II)-coordinated tetraphenylethene complex (Pt-TPPE) that exhibits strong AIECL behaviour, where the ECL signal is significantly enhanced up to 180-fold, enabling the construction of a "turn-off" ECL sensor for glutathione (GSH) detection, with high selectivity and a low detection limit of 0.298 μM.[123] Gao et al. developed organic dots based on a tert-butoxy-modified BP-DMAC molecule, achieving AIDECL by synergistically combining AIE and TADF. As shown in Fig. 12A, the modified organic dots showed 2.1-fold higher ECL efficiency than the unmodified version and were further applied in a sensitive biosensor for miR-16 detection, achieving a detection limit as low as 1.7 fM (Fig. 12B and 12C).[51] The Eu-based LMOFs, leveraging an electron-deficient boric acid group fine-tuning the ligand's energy levels for optimising triplet-state energy transfer to sensitize $Eu^{3+}$ ions, enabled strong red ECL emission. Coupled with NiFe composites as conductive carriers, the resulting biosensor demonstrated exceptional performance in detecting cytokeratin 21-1 (CYFRA 21-1), achieving a remarkably low detection limit of 0.126 pg $mL^{-1}$ and a broad linear range (0.005–100 ng $mL^{-1}$), highlighting its potential for clinical diagnostics, particularly in cancer biomarker detection.[69] Similarly, a mixed-ligand Eu-MOF achieved efficient triplet energy transfer from the ligand to the excited $Eu^{3+}$ by ligand regulation and reduced the ECL potential to as low as 0.83 V. The system integrates FeCo@CNT as a co-reaction accelerator to boost $TPrA^{\bullet}$ radical generation, and the resulting biosensor realises ultrasensitive detection of CA242, with a broad linear range (0.005–100 U $mL^{-1}$) and a low detection limit (0.0019 U $mL^{-1}$), demonstrating the potential of triplet-state-engineered MOFs in clinical diagnostics.[70]

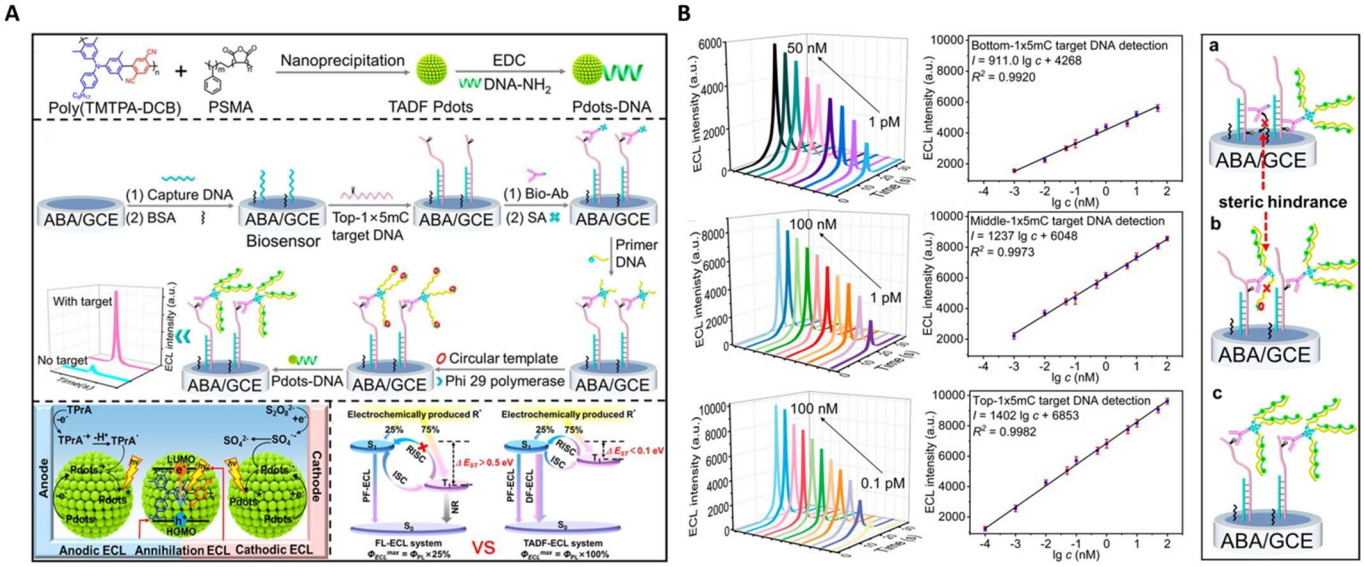



**Fig. 11** (A) Schematic diagram of Pdots-DNA preparation and ECL biosensor fabrication for DNA methylation, and ECL mechanisms. (B) ECL–time curves and calibration curves of the biosensor for DNA detection. Reproduced with permission from ref. 111. Copyright 2022 American Chemical Society.

Despite advances in designing highly emissive ECL emitters, several intrinsic challenges limit the overall efficiency of ECL systems involving triplets. For TTA-ECL, the major limitation lies in the inefficiency of TTA, combined with other loss processes, such as singlet fission and triplet quenching. For Rubrene as a typical TTA emitter, its absolute $\Phi_{ECL}$ is only around 0.1% in benzonitrile even though the triplet yield in annihilation ECL is high.[79] Additionally, triplet quenching—particularly by paramagnetic species such as radical ionscposes a significant obstacle. In energy-deficient systems, where light emission relies on TTA, achieving high ECL performance requires a delicate balance. On one hand, a high concentration of radical ions is essential to promote triplet generation through redox annihilation. On the other hand, these same radical ions can act as quenchers, suppressing triplet lifetimes and diminishing light output. Computational studies have shown that quenching-related losses can lead to ECL efficiency being underestimated by up to 20-fold in such systems.[31] In addition to energy transfer to quenchers, triplet populations may also be reduced through reactions with ground-state molecules, radicals or via extensive TTA processes, leading to the formation of exciplexes or excimers, especially for planar aromatic hydrocarbons, thereby shifting ECL emission toward longer wavelengths.[27, 124]

Another key challenge in triplet-involved ECL lies in the intrinsic instability of the radical ions that precede triplet formation. Under the anodic and cathodic extremes required for annihilation-type ECL, the electrochemically generated radical cation ($A^+$) and radical anion ($A^-$) are subjected to a combination of chemical stresses that dramatically shorten their lifetimes. The instability of radical ions is further aggravated in viscous media such as ionic liquids or polymeric matrices—despite their advantages of broad electrochemical windows and low oxygen permeability—where slow diffusion leads to prolonged residence times.[125] As a result, side reactions involving like-charged radicals or residual species with newly formed triplet excitons can kinetically compete with the desired annihilation process. These issues highlight the critical need for molecular design and system-level strategies that enhance radical stability and suppress undesired quenching pathways to fully realise triplet-based ECL emission.

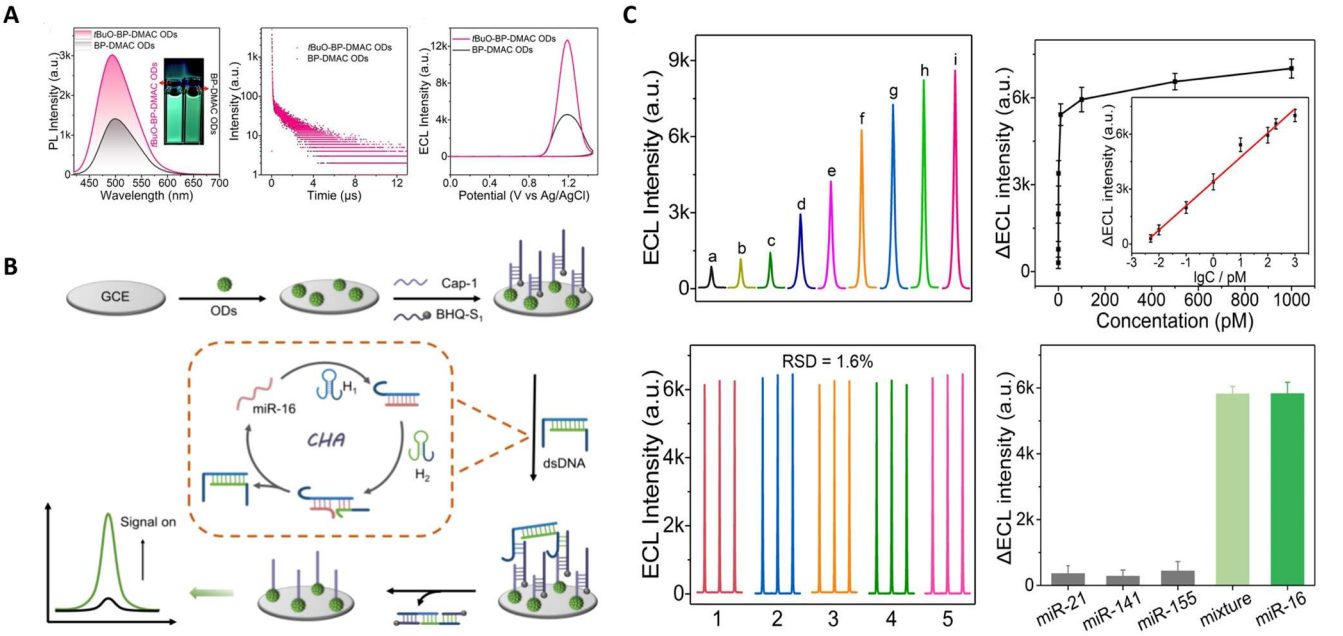



**Fig. 12** (A) Steady PL spectra, PL decay of two AIDECL-active organic dots (*t*BuOBP-DMAC ODs and BP-DMAC ODs) and ECL-potential curves of ODs-modified GCEs. (B) Scheme of ODs-based biosensor established for miR-16 detection. (C) ECL sensing performance of the developed biosensor for miR-16 detection, including concentration sensitivity, reproducibility and analyte selectivity. Reprinted with permission from ref. 51. Copyright 2024 American Chemical Society.

# 6. Summary and Outlook

The involvement of triplet states has proven to be a pivotal strategy for enhancing ECL efficiency, expanding emission lifetimes, and enabling the development of advanced ECL systems for bioanalysis, sensing, and potential use in light-emitting applications. In this review, we outlined the mechanistic pathways through which triplet excitons contribute to ECL, including triplet–triplet annihilation, thermally activated delayed fluorescence, aggregation-induced delayed fluorescence, and triplet–triplet energy transfer. We also categorised representative classes of triplet-active luminophores—spanning from metal complexes to purely organic molecules and nanostructured systems—highlighting their structure–function relationships and the design principles that facilitate triplet population and utilization.

A particular emphasis was placed on classic methods and theoretical models used to characterize triplet-state involvement in ECL processes. These include energy-sufficiency analysis, kinetic simulations and magnetic field modulation, all of which are essential for a comprehensive understanding the underlying mechanisms. However, while triplet-based ECL systems have made significant strides and are increasingly applied in areas such as ultrasensitive bioassays, mechanistic characterisation remains underexplored. Greater attention to mechanistic studies, particularly the identification and tracking of triplet intermediates, is critical for deepening our understanding and for developing next-generation ECL materials.

Looking forward, while many developments in ECL in recent decades have mirrored and drawn inspiration from the OLEDs progresses, advancing triplet-involved ECL still require several concerted efforts. First, the integration of time-resolved and in *situ* spectroelectrochemical techniques could provide real-time insights into excited-state dynamics. Second, the rational design of luminophores with tailored triplet energies, improved stability, and optimized molecular packing will be essential for practical

applications. Third, computational methods including quantum chemical calculations and kinetic modelling, should be more widely used to predict and interpret triplet behaviour. Finally, expanding triplet-based ECL to emerging platforms such as wearable diagnostics, ECL imaging, and multi-color or white-light ECL devices holds great promise. By combining mechanism-driven material design with advanced characterization and application-oriented innovation, the full potential of triplet-state processes in ECL can be more effectively harnessed.

## Acknowledgements

This research is supported by Agency for Science, Technology and Research (A*STAR) under its RIE2025 Manufacturing, Trade, and Connectivity (MTC) Programmatic Fund under grant M24M9b0013 entitled BLISS: Beyond Liquids with In-Situ Solid-state Surficial Sensorics; and the National Research Foundation Fellowship (NRF-NRFF15-2023-0011).

## Notes and references

1. s. Professor Hoijtink (Amsterdam) mentioned the results during a visit in 1963.
2. W. Miao, *Chem. Rev.*, 2008, **108**, 2506-2553.
3. L. Hu and G. Xu, *Chem. Soc. Rev.*, 2010, **39**, 3275-3304.
4. Z. Liu, W. Qi and G. Xu, *Chem. Soc. Rev.*, 2015, **44**, 3117-3142.
5. S. M. Park and D. A. Tryk, *Rev. Chem. Intermed.*, 1981, **4**, 43-79.
6. S. P. Forry and R. M. Wightman, *Electrogenerated Chemiluminescence*, Dekker, New York, 2004.
7. I. Rubinstein and A. J. Bard, *J. Am. Chem. Soc.*, 1981, **103**, 512-516.
8. H. S. White and A. J. Bard, *J. Am. Chem. Soc.*, 1982, **104**, 6891-6895.
9. J. B. Noffsinger and N. D. Danielson, *Anal. Chem.*, 1987, **59**, 865-868.
10. J. K. Leland and M. J. Powell, *J. Electrochem. Soc.*, 1990, **137**, 3127.
11. M. Yang, C. Liu, K. Qian, P. He and Y. Fang, *Analyst*, 2002, **127**, 1267-1271.
12. H. Ma-Yan, X.-W. Zheng and Z.-J. Zhang, *Chin. J. Chem* . 2004, **22**, 279-282.
13. H. Ma, X. Zheng and Z. Zhang, *Luminescence*, 2005, **20**, 303-306.
14. M. L. Calvo-Muñoz, A. Dupont-Filliard, M. Billon, S. Guillerez, G. Bidan, C. Marquette and L. Blum, *Bioelectrochemistry*, 2005, **66**, 139-143.
15. H. Yang, J. K. Leland, D. Yost and R. J. Massey, *Biotechnology (N Y)*, 1994, **12**, 193-194.
16. N. P. Sardesai, J. C. Barron and J. F. Rusling, *Anal. Chem.*, 2011, **83**, 6698-6703.
17. R. Kurita, K. Arai, K. Nakamoto, D. Kato and O. Niwa, *Anal. Chem.*, 2012, **84**, 1799-1803.
18. C.-K. Moon and M. C. Gather, *Adv. Opt. Mater.*, 2024, **12**, 2401253.
19. L. R. Faulkner and D. J. Freed, *J. Am. Chem. Soc.*, 1971, **93**, 2097-2102.
20. L. R. Faulkner and D. J. Freed, *J. Am. Chem. Soc.*, 1971, **93**, 3565-3568.
21. N. E. Tokel and A. J. Bard, *J. Am. Chem. Soc.*, 1972, **94**, 2862-2863.
22. *Journal*, G. J. Hoijtink suggested triplet generation followed by triplettriplet annihilation as a possible light-emitting process for the anioncation annihilation reaction, at the “Symposium on Chemiluminescence,” Durham, N. C., 1965.
23. D. L. Maricle and A. Maurer, *J. Am. Chem. Soc.*, 1967, **89**, 188-189.
24. J. Chang, D. M. Hercules and D. K. Roe, *Electrochim. Acta*, 1968, **13**, 1197-1207.
25. T. C. Werner, J. Chang and D. M. Hercules, *J. Am. Chem. Soc.*, 1970, **92**, 763-768.
26. D. L. Akins and R. L. Birke, *Chem. Phys. Lett.*, 1974, **29**, 428-435.
27. J. B. Ketter and R. M. Wightman, *J Am Chem Soc*, 2004, **126**, 10183-10189.
28. E. W. Grabner and E. Brauer, *Ber. Bunsenges. Phys. Chem.*, 1972, **76**, 106-110.
29. M. Libert and A. J. Bard, *J. Electrochem. Soc.*, 1976, **123**, 814.

30. P. R. Michael and L. R. Faulkner, *J. Am. Chem. Soc.*, 1977, **99**, 7754-7761.
31. E. L. Ritchie, P. Pastore and R. M. Wightman, *J. Am. Chem. Soc.*, 1997, **119**, 11920-11925.
32. E. M. Gross, J. D. Anderson, A. F. Slaterbeck, S. Thayumanavan, S. Barlow, Y. Zhang, S. R. Marder, H. K. Hall, M. F. Nabor, J. F. Wang, E. A. Mash, N. R. Armstrong and R. M. Wightman, *J. Am. Chem. Soc.*, 2000, **122**, 4972-4979.
33. A. Elangovan, H.-H. Chiu, S.-W. Yang and T.-I. Ho, *Org. Biomol. Chem.*, 2004, **2**, 3113-3118.
34. A. Elangovan, J.-H. Lin, S.-W. Yang, H.-Y. Hsu and T.-I. Ho, *J. Org. Chem.*, 2004, **69**, 8086-8092.
35. R. Ishimatsu, H. Shintaku, C. Adachi, K. Nakano and T. Imato, *ChemistrySelect*, 2017, **2**, 10531-10536.
36. R. Ishimatsu, S. Matsunami, T. Kasahara, J. Mizuno, T. Edura, C. Adachi, K. Nakano and T. Imato, *Angew. Chem. Int. Ed.*, 2014, **53**, 6993-6996.
37. H. Uoyama, K. Goushi, K. Shizu, H. Nomura and C. Adachi, *Nature*, 2012, **492**, 234-238.
38. T. Pizza, A. Capobianco and A. Troisi, *J. Phys. Chem. Lett.*, 2025, **16**, 3056-3062.
39. L. G. Franca, D. G. Bossanyi, J. Clark and P. L. dos Santos, *ACS Appl. Opt. Mater.*, 2024, **2**, 2476-2500.
40. P. Huang, B. Zhang, Q. Hu, B. Zhao, Y. Zhu, Y. Zhang, Y. Kong, Z. Zeng, Y. Bao, W. Wang, Y. Cheng and L. Niu, *ChemPhysChem*, 2021, **22**, 726-732.
41. Z. Zeng, P. Huang, Y. Kong, L. Tong, B. Zhang, Y. Luo, L. Chen, Y. Zhang, D. Han and L. Niu, *Chem. Commun.*, 2021, **57**, 5262-5265.
42. S. Carrara, A. Aliprandi, C. F. Hogan and L. De Cola, *J. Am. Chem. Soc.*, 2017, **139**, 14605-14610.
43. X. Wei, M.-J. Zhu, H. Yan, C. Lu and J.-J. Xu, *Chem. Eur. J.*, 2019, **25**, 12671-12683.
44. H. Jiang, Z. Qin, Y. Zheng, L. Liu and X. Wang, *Small*, 2019, **15**, 1901170.
45. J.-L. Liu, J.-Q. Zhang, Z.-L. Tang, Y. Zhuo, Y.-Q. Chai and R. Yuan, *Chem. Sci.*, 2019, **10**, 4497-4501.
46. Z. Han, Y. Zhang, Y. Wu, Z. Li, L. Bai, S. Huo and X. Lu, *Anal. Chem.*, 2019, **91**, 8676-8682.
47. X. Wei, M.-J. Zhu, Z. Cheng, M. Lee, H. Yan, C. Lu and J.-J. Xu, *Angew. Chem. Int. Ed.*, 2019, **58**, 3162-3166.
48. H. Peng, Z. Huang, H. Deng, W. Wu, K. Huang, Z. Li, W. Chen and J. Liu, *Angew. Chem. Int. Ed.*, 2020, **59**, 9982-9985.
49. B. Zhang, Y. Kong, H. Liu, B. Chen, B. Zhao, Y. Luo, L. Chen, Y. Zhang, D. Han, Z. Zhao, B. Z. Tang and L. Niu, *Chem. Sci.*, 2021, **12**, 13283-13291.
50. H. Gao, S.-Y. Shi, S.-M. Wang, Q.-Q. Tao, H.-L. Ma, J. Hu, H.-Y. Chen and J.-J. Xu, *Aggregate*, 2024, **5**, e394.
51. H. Gao, Y.-L. Jia, J.-B. Lin, S.-M. Wang, Z.-Y. Lin, H.-L. Ma, H.-Y. Chen and J.-J. Xu, *Anal. Chem.*, 2024, **96**, 7780-7786.
52. X. R. Zhang, W. R. G. Baeyens, G. Van Der Weken, A. C. Calokerinos and K. Nakashima, *Anal. Chim. Acta*, 1995, **303**, 121-125.
53. F. Yang, C. Zhang, W. R. Baeyens and X. Zhang, *J. Pharm. Biomed. Anal.*, 2002, **30**, 473-478.
54. X. F. Yang and H. Li, *Talanta*, 2004, **64**, 478-483.
55. Y.-D. Liang, J.-F. Song and X.-F. Yang, *Anal. Chim. Acta*, 2004, **510**, 21-28.
56. G. Porter and F. Wilkinson, *Proc. R. Soc. Lond. Ser. A.*, 1961, **264**, 1-18.
57. S. M. Park and A. J. Bard, *Chem. Phys. Lett.*, 1976, **38**, 257-262.
58. Q. Li, C. Zhang, J. Y. Zheng, Y. S. Zhao and J. Yao, *Chem. Commun.*, 2012, **48**, 85-87.
59. H. Minami, T. Ichikawa, K. Nakamura and N. Kobayashi, *Chem. Commun.*, 2019, **55**, 12611-12614.
60. R. Ozawa, H. Minami, K. Nakamura and N. Kobayashi, *J. Mater. Chem. C.*, 2021, **9**, 2252-2257.
61. M. Zhang, C. Zhang and H. Qi, *Mikrochim. Acta*, 2004, **144**, 155-160.
62. Y. Liu, S. Chen, H. Zhao and L. Jin, *Anal. Sci.*, 2005, **21**, 373-375.
63. S.-L. Chen, Y. Liu, H.-C. Zhao, L.-P. Jin, Z.-L. Zhang and Y.-Z. Zheng, *Luminescence*, 2006, **21**, 20-25.
64. Y.-D. Liang, W. Gao and J.-F. Song, *Bioorg. Med. Chem. Lett.*, 2006, **16**, 5328-5333.
65. R. E. Whan and G. A. Crosby, *J. Mol. Spectrosc.*, 1962, **8**, 315-327.
66. P. R. Selvin, *Nat. Struct. Biol.*, 2000, **7**, 730-734.
67. B. D. Chandler, D. T. Cramb and G. K. H. Shimizu, *J. Am. Chem. Soc.*, 2006, **128**, 10403-10412.
68. Y. Cui, Y. Yue, G. Qian and B. Chen, *Chem. Rev.*, 2012, **112**, 1126-1162.
69. Y. Wang, G. Zhao, H. Chi, S. Yang, Q. Niu, D. Wu, W. Cao, T. Li, H. Ma and Q. Wei, *J. Am. Chem. Soc.*, 2021, **143**, 504-512.
70. H. Dong, S. Liu, Q. Liu, Y. Li, Z. Xu, Y. Li and Q. Wei, *Anal. Chem.*, 2022, **94**, 12852-12859.

71. H. Li, S. Voci, A. Wallabregue, C. Adam, G. M. Labrador, R. Duwald, I. Hernández Delgado, S. Pascal, J. Bosson, J. Lacour, L. Bouffier and N. Sojic, *ChemElectroChem*, 2017, **4**, 1750-1756.
72. A. Zweig and D. L. Maricle, *J. Phys. Chem.*, 1968, **72**, 377-378.
73. D. J. Freed and L. R. Faulkner, *J. Am. Chem. Soc.*, 1972, **94**, 4790-4792.
74. W. M. Schwarz and I. Shain, *J. Phys. Chem.*, 1965, **69**, 30-40.
75. K. S. V. Santhanam and A. J. Bard, *J. Am. Chem. Soc.*, 1965, **87**, 139-140.
76. S. W. Feldberg, *J. Am. Chem. Soc.*, 1966, **88**, 390-393.
77. S. W. Feldberg, *J. Phys. Chem.*, 1966, **70**, 3928-3930.
78. R. Bezman and L. R. Faulkner, *J. Am. Chem. Soc.*, 1972, **94**, 3699-3707.
79. R. Bezman and L. R. Faulkner, *J. Am. Chem. Soc.*, 1972, **94**, 6324-6330.
80. M. M. Collinson and R. M. Wightman, *Anal. Chem.*, 1993, **65**, 2576-2582.
81. C. P. Keszthelyi, H. Tachikawa and A. J. Bard, *J. Am. Chem. Soc.*, 1972, **94**, 1522-1527.
82. R. C. Johnson, R. E. Merrifield, P. Avakian and R. B. Flippen, *Phys. Rev. Lett.*, 1967, **19**, 285-287.
83. P. Avakian and R. E. and Merrifield, *Mol. Cryst.*, 1968, **5**, 37-77.
84. R. E. Merrifield, *J. Chem. Phys.*, 1968, **48**, 4318-4319.
85. L. R. Faulkner and A. J. Bard, *J. Am. Chem. Soc.*, 1969, **91**, 209-210.
86. L. R. Faulkner and A. J. Bard, *J. Am. Chem. Soc.*, 1969, **91**, 6495-6497.
87. L. R. Faulkner and A. J. Bard, *J. Am. Chem. Soc.*, 1969, **91**, 6497-6498.
88. L. R. Faulkner, H. Tachikawa and A. J. Bard, *J. Am. Chem. Soc.*, 1972, **94**, 691-699.
89. N. Periasamy, S. J. Shah and K. S. V. Santhanam, *J. Chem. Phys.*, 1973, **58**, 821-823.
90. H. Tachikawa and A. J. Bard, *Chem. Phys. Lett.*, 1974, **26**, 10-15.
91. H. Tachikawa and A. J. Bard, *Chem. Phys. Lett.*, 1974, **26**, 568-573.
92. H. Pan, Y. Shen, H. Wang, L. He and B. Hu, *Sci. Rep.*, 2015, **5**, 9105.
93. H. Pan, Y. Shen, L. Luan, K. Lu, J. Duan and B. Hu, *J. Phys. Chem. C*, 2015, **119**, 8089-8094.
94. H. Pan, J. Zhou and S. Liu, *J. Phys. Chem. C*, 2023, **127**, 17432-17437.
95. S. Kumar, P. Tourneur, J. R. Adsetts, M. Y. Wong, P. Rajamalli, D. Chen, R. Lazzaroni, P. Viville, D. B. Cordes, A. M. Z. Slawin, Y. Olivier, J. Cornil, Z. Ding and E. Zysman-Colman, *J. Mater. Chem. C.*, 2022, **10**, 4646-4667.
96. Y. Luo, B. Zhao, B. Zhang, Y. Lan, L. Chen, Y. Zhang, Y. Bao and L. Niu, *Analyst*, 2022, **147**, 2442-2451.
97. R. E. Visco and E. A. Chandross, *Electrochim. Acta*, 1968, **13**, 1187-1196.
98. G. J. Hoytink, *Disc. Faraday Soc.*, 1968, **45**, 14-22.
99. C. A. Parker and G. D. Short, *Trans. Faraday Soc.*, 1967, **63**, 2618-2622.
100. E. W. Grabner and E. Brauer, *Ber. Bunsenges. Phys. Chem.*, 1972, **76**, 111-114.
101. G. Valenti, C. Bruno, S. Rapino, A. Fiorani, E. A. Jackson, L. T. Scott, F. Paolucci and M. Marcaccio, *J. Phys. Chem. C*, 2010, **114**, 19467-19472.
102. J. Gu, Y. Gao, J. Wu, Q. Li, A. Li, W. Zhang, H. Dong, B. Wen, F. Gao and Y. S. Zhao, *ACS Appl. Mater. Interfaces.*, 2017, **9**, 8891-8899.
103. J. Wei, N. Yang, F. Li, S. Cai, B. Zhang and Z. Cai, *Chem. Eur. J.*, 2024, **30**, e202401036.
104. X. Cao, D. Zhang, S. Zhang, Y. Tao and W. Huang, *J. Mater. Chem. C.*, 2017, **5**, 7699-7714.
105. R. Ishimatsu, T. Edura, C. Adachi, K. Nakano and T. Imato, *Chem. Eur. J.*, 2016, **22**, 4889-4898.
106. A. Fracassa, F. Calogero, G. Pavan, P. Nikolaou, A. Fermi, P. Ceroni, F. Paolucci, P. G. Cozzi, T. Scattolin, N. Demitri, F. Negri, A. Gualandi, A. Aliprandi and G. Valenti, *Chem. Sci.*, 2024, **15**, 17892-17899.
107. S. Kumar, L. G. Franca, K. Stavrou, E. Crovini, D. B. Cordes, A. M. Z. Slawin, A. P. Monkman and E. Zysman-Colman, *J. Phys. Chem. Lett.*, 2021, **12**, 2820-2830.
108. K. Chu, Z. Ding and E. Zysman-Colman, *Chem. Eur. J.*, 2023, **29**, e202301504.
109. F. Zheng, M. Liu, Y. Li, J. Wei, X. Chen, J. Ni and Z. Cai, *ACS Appl. Opt. Mater.*, 2025, **3**, 240-247.
110. J. Wei, M. Liu, S.-J. Lin and Z. Cai, *J. Phys. Chem. Lett.*, 2024, **15**, 11104-11111.
111. C. Wang, J. Wu, H. Huang, Q. Xu and H. Ju, *Anal. Chem.*, 2022, **94**, 15695-15702.
112. L. Yang, L. Dong, D. Hall, M. Hesari, Y. Olivier, E. Zysman-Colman and Z. Ding, *SmartMat*, 2023, **4**, e1149.
113. X. Zhou, J. Cheng and H. Wang, *Molecules*, 2025, **30**, 1718.
114. J. I. Lee, H. Choi, S. H. Kong, S. Park, D. Park, J. S. Kim, S. H. Kwon, J. Kim, S. H. Choi, S. G. Lee, D. H. Kim and M. S. Kang, *Adv. Mater.*, 2021, **33**, 2100321.

115. D.-K. Kwon and J.-M. Myoung, *Chem. Eng. J.*, 2020, **379**, 122347.
116. J.-W. Oh, J.-Y. Jeong, T.-Y. Eom, S.-D. Baek and J.-M. Myoung, *Chem. Eng. J.*, 2021, **416**, 129202.
117. S. Lee, H. J. Lee, Y. Ji, K. H. Lee and K. Hong, *Adv. Mater.*, 2021, **33**, 2005456.
118. Y. K. Cho, H. Kim, A. Bénard, H.-K. Woo, F. Czubayko, P. David, F. J. Hansen, J. I. Lee, J. H. Park, E. Schneck, G. F. Weber, I.-S. Shin and H. Lee, *Sci. Adv.*, 2022, **8**, eabq4022.
119. H. Yee, K. Jung, J. Park, W. Choi, N. H. Kim, J. Kim and M. S. Kang, *Adv. Funct. Mater.*, 2025, **35**, 2417514.
120. Q. Han, C. Wang, P. Liu, G. Zhang, L. Song and Y. Fu, *Chem. Eng. J.*, 2021, **421**, 129761.
121. X. Zou, Z. Zeng, B. Zhao, Y. Yue, Z. Xu, Y. Zhang, Y. Fu, Z. Xie, L. Niu and B. Zhang, *ACS Appl. Polym. Mater.*, 2023, **5**, 10116-10126.
122. J. Liu, L. Yang, S. Li, K. Zhang, X. Zhou, G. Li, L. Wu and Y. Qin, *Biosens. Bioelectron.*, 2024, **251**, 116103.
123. L. He, Y. Wang, Y. Wang, Y. Niu, N. Li, J. Ye and Y. Ma, *Electrochim. Acta*, 2024, **475**, 143596.
124. C. A. Parker and T. A. Joyce, *Chem. Commun. (London)*, 1967, **15**, 744-745.
125. R. Ishimatsu, *Anal. Sci.*, 2025, **41**, 511-522.